Research in Pharmaceutical Sciences, August 2025; 20(4): 610-634
Received: 02-04-2025
Peer Reviewed: 15-05-2025
Revised: 28-06-2025
Accepted: 14-07-2025
Published: 25-08-2025

School of Pharmacy & Pharmaceutical Sciences
Isfahan University of Medical Sciences

Original Article

Development and evaluation of gelatin/hyaluronic acid nanofibrous dressing loaded with silver nanoparticles and phenytoin for enhanced wound healing: an *in-vitro* and *in-vivo* study

Jaber Emami[1,*], Niloofar Mostolizadeh[1], Majid Tabbakhian[1], Parisa Heydari[2], Anousheh Zargar Kharazi[2], Mohsen Minaeiyan[3], Farshid Hasanzadeh[4], Mina Mirian[5], and Ardeshir Talebi[6]

[1]*Department of Pharmaceutics, School of Pharmacy and Pharmaceutical Sciences, Isfahan University of Medical Sciences, Isfahan, I.R. Iran.*
[2]*Department of Biomaterials, Tissue Engineering and Nanotechnology, School of Advanced Technologies in Medicine, Isfahan University of Medical Sciences, Isfahan, I.R. Iran.*
[3]*Department of Pharmacology and Toxicology, School of Pharmacy and Pharmaceutical Sciences, Isfahan University of Medical Sciences, Isfahan, I.R. Iran.*
[4]*Department of Medical Chemistry, School of Pharmacy and Pharmaceutical Sciences, Isfahan University of Medical Sciences, Isfahan, I.R. Iran.*
[5]*Department of Pharmaceutical Biotechnology, School of Pharmacy and Pharmaceutical Sciences, Isfahan University of Medical Sciences, Isfahan, I.R. Iran.*
[6]*Department of Pathology, School of Medicine, Isfahan University of Medical Sciences, Isfahan, I.R. Iran.*

Abstract

Background and purpose: Wound dressings are essential in managing chronic wounds like pressure ulcers, which increase healthcare costs and hospital stays. There is a rising demand for advanced dressings that effectively promote healing. This study developed electrospun gelatin-hyaluronic acid (Gel/HA) nanofibers loaded with silver nanoparticles (Ag NPs) and phenytoin to enhance wound healing.
Experimental approach: Ag NPs were synthesized via silver nitrate reduction using trisodium citrate and tannic acid, and characterized for size, zeta potential, PDI, UV-Vis absorption, and XRD patterns. Drug-free and drug-loaded Gel/HA nanofibers were fabricated and analyzed using FE-SEM, FTIR, DSC, XRD, swelling behavior, drug loading, and release profiles. In vitro antibacterial and in vivo wound healing studies were conducted.
Findings/Results: Optimized Ag NPs had a size of 41.96 ± 1.2 nm, zeta potential of −23.77 ± 1.31 mV, and PDI of 0.35 ± 0.02. The ideal nanofiber formulation (20 g Gel and 0.25 g HA/100 mL) showed drug loading efficiencies of 56.02 ± 1.8% (Ag NPs) and 61.02 ± 2.82% (phenytoin), with release times of 22.23 and 28.53 h, respectively. The nanofibers demonstrated high swelling (822.2%) and strong antibacterial activity. In vivo studies revealed significantly faster wound closure, improved epithelialization, collagen deposition, and complete healing within 15 days. These effects reflect the synergy between Ag NPs' antimicrobial and phenytoin's regenerative properties.
Conclusion and implications: Gel/HA nanofibers loaded with Ag NPs and phenytoin show great promise as advanced wound dressings. Further studies in larger animal models and clinical trials are warranted.

Keywords: Gelatin; Hyaluronic acid; Nanofibers; Phenytoin; Silver nanoparticles; Wound healing.

INTRODUCTION

The skin, as one of the largest and most complex organs in the human body, comprises multiple layers, the outermost of which is known as the epidermis. The epidermis is susceptible to external destructive actions, resulting in various types of ulcers and injuries, including chronic wounds such as bedsores and pressure ulcers (1).

*Corresponding author: J. Emami
Tel: +98-3137927111, Fax: +98-3136680011
Email: emami@pharm.mui.ac.ir

Access this article online
Website: http://rps.mui.ac.ir
DOI: 10.4103/RPS.RPS_60_25

These injuries present a challenge in clinical settings due to their susceptibility to infection and delayed healing. A wound bed, with its warm, wet, and nutrient-rich environment, is an ideal setting for microbial growth, which complicates the healing process and necessitates special attention to prevent infection and optimize recovery (2,3).

Wound dressings are crucial in the healing process as they provide a barrier against microorganisms, protect the wound from external contaminants, and create an optimal environment for tissue regeneration (4,5). However, despite the availability of over 300 types of wound dressings, choosing the most appropriate one remains a critical issue. Not all wounds require the same dressing type, and the ideal dressing should maintain a moist environment while preventing microbial invasion and supporting tissue healing (6,7). This has prompted the exploration of biopolymers such as gelatin (Gel) and hyaluronic acid (HA), which offer unique properties that can aid in wound healing.

Gelatin, derived from collagen, is highly hydrophilic, making it an excellent candidate for maintaining moisture in the wound bed, which is essential for promoting healing. Its fast degradability allows for easy absorption by the body, thus avoiding any negative long-term effects. However, its lack of antimicrobial properties makes it vulnerable to infections in wound sites, necessitating the incorporation of additional materials to enhance its functionality (8,9).

On the other hand, HA, a naturally occurring polymer, has remarkable biological properties, including the ability to promote tissue regeneration, reduce inflammation, and enhance collagen synthesis. HA's hemostatic properties are also beneficial in wound healing (10,11). However, it is not without limitations. HA's high cost and potential instability in certain environmental conditions make it challenging to use on its own as a wound dressing material (12). Together, Gel and HA can form a synergistic system that combines moisture retention with regenerative capabilities, but their efficacy is often enhanced when combined with other materials such as nanoparticles.

Silver nanoparticles (Ag NPs) have attracted significant attention due to their broad-spectrum antibacterial properties, which are particularly effective in preventing microbial infections in wound care (13-15). The unique properties of Ag NPs, including their large surface area and high reactivity, make them effective in disrupting bacterial cell walls and inhibiting microbial growth (16,17). However, the use of Ag NPs also has some challenges. Potential toxicity to human cells, particularly at higher concentrations, remains a concern, though recent advancements in controlled-release formulations help mitigate these risks (18,19). Moreover, Ag NPs can interact with the wound site to release silver ions gradually, which aids in promoting faster tissue regeneration and reducing infection risk (20,21).

Phenytoin, an anticonvulsant medication, has been found to accelerate wound healing by promoting collagen synthesis, new vascular formation, and tissue regeneration (22). In topical formulations, phenytoin has shown significant improvement in healing traumatic wounds, burns, and bedsores. When applied to wounds, it has been observed to enhance tissue regeneration by reducing inflammation and encouraging faster recovery of the wound site (23). However, phenytoin, while beneficial, also poses challenges in terms of its controlled release and bioavailability, which may require effective delivery systems such as nanofibers to optimize its therapeutic potential.

Among the various techniques for fabricating wound dressings, electrospinning has emerged as one of the most promising methods for producing nanofibers (24,25). Electrospun nanofibers, with diameters ranging from nanometers to microns, exhibit unique properties, including high surface area, porosity, and the ability to mimic the natural extracellular matrix (7). These properties make them ideal for use in wound care, as they allow for controlled drug release, oxygen permeability, and moisture retention, all essential qualities for an optimal dressing. Additionally, the scalability and ease of fabrication of electrospun nanofibers make them highly suitable for industrial-scale production. However, like all materials,

electrospun nanofibers have their limitations. The mechanical stability of nanofibers may be insufficient for certain applications, and their degradability must be carefully controlled to avoid premature disintegration in wound environments (26).

Recent studies have highlighted the advantages of incorporating metal nanoparticles into electrospun nanofibers. These particles enhance the antibacterial activity of the nanofibers while also contributing to wound-healing processes. Recent research has explored the development of bioactive nanofibrous matrices capable of sustained drug release, providing enhanced antimicrobial and healing effects in wound environments. Incorporating agents like Ag NPs and phenytoin into these matrices can significantly improve antibacterial activity and promote faster wound healing, making electrospun nanofibers a promising avenue for future wound care solutions (4,27,28).

This study explores the potential of electrospun nanofibers as advanced wound dressings by incorporating Ag NPs and phenytoin, aiming to enhance their antibacterial properties and promote more effective wound healing. We propose that the integration of these biopolymers and nanoparticles will enhance wound closure efficiency, accelerate tissue regeneration, and decrease the risk of infection, presenting a viable alternative to traditional wound care solutions. This study will assess the mechanical characteristics, biodegradability, and controlled release profiles of the developed dressings to confirm their appropriateness for practical applications.

MATERIALS AND METHODS

Materials

Bovine gel type A from Kanto, Japan; HA (average molecular weight = 250 kDa), from Solarbio, China; from Alhavi, Iran; glyoxal and trisodium citrate dihydrate from Samsung, Korea. Silver nitrate ($AgNO_3$; 99%) from Junsei, Japan; tannic acid from Alfa Aesar, UK; acetic acid glacial 100%, nitric acid 65%, Mueller Hinton agar, and Mueller Hinton broth media from Merck, Germany. The Pasteur Institute of Iran (Tehran) provided *Staphylococcus aureus* and *Pseudomonas aeruginosa*. The remainder of the chemical compounds employed in this investigation were analytical grade.

Ag NPs preparation

The trisodium citrate reduction technique was employed to fabricate Ag NPs. First, 85 mg of $AgNO_3$, 129 mg of trisodium citrate, and 21.25 mg of tannic acid were dissolved in 90 mL, 5 mL, and 5 mL of deionized water, respectively. The $AgNO_3$ solution was heated until it began to boil. Once boiling, the trisodium citrate and tannic acid solutions were combined and added dropwise to the boiling $AgNO_3$ solution. The heating was continued until a dark brown color appeared, indicating the reduction of Ag^+ ions. The solution was then heated for an additional 15 min before being cooled to room temperature using an ice-water bath (29,30). Finally, the mixture was thoroughly suspended and centrifuged for 10 min at 12,000 rpm to separate the dry material. A Zeta Sizer was used to determine the particle size (PS), zeta potential (ZP), and polydispersity index (PDI). UV-visible spectroscopy was employed as one of the most effective analytical methods for identifying the structure of the Ag NPs. Field-emission scanning electron microscopy (FE-SEM) was used to examine the morphology of the Ag NPs.

Electrospinning process

Gel/HA nanofibers and Gel/HA nanofibers loaded with phenytoin and Ag NPs were produced using an electrospinning process. Initially, 2 g of pure Gel was dissolved in a 10 mL mixture of acetic acid and water (7:3) with moderate stirring at 40 °C for 40 min. Subsequently, 0.015 g, 0.025 g, and 0.035 g of HA were individually dissolved in three separate 10 mL volumes of the Gel solution, respectively (31). The chemical production of phenytoin-Ag NPs-loaded nanofibers utilized passive loading of phenytoin and Ag nanoparticles. This method involved the incorporation of 0.5% w/v produced Ag NPs and 0.5% w/v phenytoin into the Gel/HA solution, which had previously been disseminated or dissolved in acetic acid. The mixture was stirred in obscurity at 40 °C for a

minimum duration of 5 h. Glyoxal, a non-toxic and fluorine-free cross-linking agent, was employed for *in-situ* cross-linking during electrospinning. Before the electrospinning process, 0.0917% w/w glyoxal (estimated from the weight of the Gel powder) was integrated into the optimum solution (32).

The electrospinning procedure was subsequently done to produce the nanofibers. A counter electrode was positioned 20 cm from the capillary tip, and a voltage of 25 kV was applied. The polymer solution was fed into the electrospinning apparatus using a syringe pump set at a flow rate of 0.66 mL/h. All studies were performed at ambient temperature, and the nanofibers were gathered on aluminum foil (33).

Characterization of electrospinning wound dressing

FE-SEM was employed to examine the morphological properties of the electrospun nanofibers. A minor portion of the fibers was sputter-coated with platinum and affixed to an SEM sample holder. Imaging was performed at an accelerating voltage of 20 kV. The mean fiber diameter was ascertained by analyzing a minimum of one hundred individual fibers with ImageJ software, a well-established image analysis tool (34).

Fourier-transform infrared (FTIR) spectra of the nanofibers were recorded to evaluate the chemical structural alterations in the Gel/HA matrix after adding Ag NPs and phenytoin. To prepare the samples, the fibers underwent a grinding process to reduce them to small fragments. These fragments were then combined with potassium bromide (KBr) to form pellets. FTIR measurements were performed in the wavenumber range of 4000-800 cm^{-1} with a resolution of 2 cm^{-1}. The thermal behavior was examined using differential scanning calorimetry (DSC). Approximately 3-5 mg of the material was heated in a nitrogen environment at a rate of 10 °C/min, ranging from 30 °C to 300 °C. X-ray powder diffraction (XRD) analysis was conducted to identify the structural phase of the Ag NPs before and after electrospinning. The diffraction patterns displayed distinct peaks at 2θ = 38° and 46°, indicative of the crystalline planes of Ag NPs, hence affirming their crystalline structure (35).

Ag NP's and phenytoin's entrapment efficiency

The entrapment efficiency of Ag NPs in nanofibers is measured by the digestion of six nanofiber mats (1.5 × 1.5 cm^2) in water-nitric acid (7:3). Atomic absorption spectroscopy was used to determine the Ag concentration. The following equation was used to compute the entrapment efficiency (36):

$$\text{Entrapment efficiency of silver (\%)} = \frac{\text{Mass silver (1.5 cm}^2\text{)} \times \text{total mat area}}{\text{Mass of total silver initially added}} \quad (1)$$

The entrapment efficiency of phenytoin in nanofibers was determined by the digestion of six nanofiber mats (1.5 × 1.5 cm^2) in water-ethanol (1:9). The concentration of phenytoin was determined using a UV spectrophotometer set to 218 nm. The following equation is used to compute the entrapment efficiency (37):

$$\text{Entrapment efficiency of phenytoin sodium} = \frac{\text{Mass of phenytoin in (1.5 cm}^2\text{ mat)} \times \text{total mat area}}{\text{Mass of total phenytoin initially added}} \quad (2)$$

Degree of swelling

The following equation was used to compute the degrees of swelling of the manufactured nanofiber wound dressing:

$$\text{Degree of swelling} = \frac{M - M_d}{M_d} \quad (3)$$

where M is the weight of a swelled nanofibers sample that has been wiped dry with filter paper, and M_d is the sample's starting weight. For periods of 2, 4, 8, 24, and 48 h, the test was carried out in phosphate-buffered saline (PBS), pH 7.4, at 37 °C (38).

In-vitro release studies of phenytoin

A known amount of phenytoin-loaded nanofiber was placed in a dialysis bag to determine the concentration of phenytoin released from the electrospun HA/Gel nanofibers. The dialysis bag was then submerged in 20 mL of PBS (pH 7.4) containing 10% ethanol. The experiment was conducted on a heated stirrer at 37 °C and 100 RPM. Samples were withdrawn at specified intervals (0, 1, 2, 3, 4, 8, 24, 48, and 72 h). The released phenytoin concentration was analyzed using a UV-Vis spectrophotometer set to 234 nm. The release experiment was performed in triplicate, and the average data are presented as percentage release (37).

To evaluate the colloidal stability of the Ag NPs, the prepared suspensions were stored at ambient temperature and monitored over four weeks. No visible aggregation or sedimentation was detected, and the UV-Vis absorption peak at ~423 nm showed no significant shift, confirming the stability of the nanoparticles during the storage period.

In-vitro release studies of Ag NPs

To determine the concentration of Ag ions released from Ag NPs-loaded HA/Gel nanofibers, a known quantity of the nanofibers was immersed in 20 mL of PBS (pH 7.4). The release experiments were performed in a thermostatically controlled shaking water bath at 37 °C and 100 rpm. At predetermined time intervals (0, 1, 2, 3, 4, 8, 24, 48, and 72 h), 1 mL samples were withdrawn. After adding 300 µL of nitric acid to each sample and vortexing, the samples were incubated in a thermostatically controlled shaking incubator at 40 °C for 24 h. An equivalent volume of fresh medium was added to maintain the sink condition. The release experiment was repeated three times, and the average data are presented as the percentage of release (17).

Antibacterial assay

Anti-bacterial effect of Ag NPs

The antibacterial efficacy of Ag NPs against *S. aureus* and *P. aeruginosa* was assessed in the Mueller-Hinton broth medium. Ag NPs, within their concentration range (3-283 µg/mL), were systematically tested in the microplate wells. The microplate also included three wells with bacterial suspension (1.5×10^5 CFU/mL) without treatment (growth control) and three wells containing only the medium (background control). Optical densities (ODs) were measured using a microplate reader at 540 nm for 24 h at 37 °C. The minimum inhibitory concentration (MIC) of Ag NPs was determined by calculating the growth percentage for each treatment, using the equation below. Optical density readings were calculated by subtracting the background ODs from bacterial cell-free wells and evaluating % bacteria growth according to the following equation:

$$\text{Growth (\%)} = \frac{OD_{595} \text{ of wells containing the test}}{OD_{595} \text{ of the drug} - \text{free well}} \times 100 \quad (4)$$

All experiments were conducted in triplicate, and the results are presented as mean values (39).

Antibacterial efficacy of Gel/HA nanofibers containing Ag NPs and phenytoin using the colony-counting method

The colony-counting method was employed to evaluate the antibacterial activity of Gel/HA nanofibers loaded with Ag NPs and phenytoin against *S. aureus* and *P. aeruginosa*. Different weights of Gel/HA nanofibers were thoroughly dissolved in 1 mL of sterile water. To this, 8 mL of Minton Hinton Broth and 1 mL of bacterial suspension (1.5×10^5 CFU/mL) were added, and the mixture was vortexed well. The resulting solution was incubated for 24 h at 37 °C in a shaking incubator. Following incubation, 100 µL of bacterial culture was spread onto Muller-Hinton agar plates using a surface-spreading method. The plates were then incubated at 37 °C for 24 h. Each experiment was performed in triplicate (40).

Antibacterial assay of Gel/HA nanofibers containing Ag NPs and phenytoin using the disc diffusion method

The antibacterial activity of Gel/HA nanofibers loaded with Ag NPs and phenytoin was assessed qualitatively using the disc diffusion method to determine the zone of inhibition against *S. aureus* and *P. aeruginosa*. Bacterial suspensions (1.5×10^5 CFU/mL) were cultured on Muller-Hinton agar plates. Ciprofloxacin discs were used as a positive control, while Gel/HA nanofibers without additives served as a negative control. Gel/HA nanofibers containing Ag NPs and phenytoin were tested as the experimental samples. The culture plates were incubated at 37 °C for 24 h. After incubation, the zone of inhibition around each disc was measured. Each experiment was conducted in triplicate, and the results are presented as mean values (41).

Antibacterial assay of Gel/HA nanofibers containing Ag NPs and phenytoin using the plate well method

The antibacterial activity of Gel/HA nanofibers stabilized with Ag NPs and phenytoin against *S. aureus* and *P. aeruginosa* was evaluated using the plate well method. Wells were created in the agar medium by forming indentations with the broad end of a Pasteur pipette tip and removing the agar plug. After the medium solidified, the bacterial suspension (1.5×10^5 CFU/mL) was spread evenly on the surface of the agar, and the wells were formed. A single drop of the Gel/HA-stabilized Ag NPs solution was added to each well. The plates were then incubated at 37 °C for 24 h. Ag NPs alone were used as a positive control. All experiments were performed in triplicate, and the results are expressed as mean values (42).

In-vivo evaluation of Gel/HA nanofibers containing Ag NPs and phenytoin (wound-healing study in Wistar rats)

The *in vivo* studies were conducted under the ethical guidelines set by the Animal Research Ethics Committee of Isfahan University of Medical Sciences and the National Institutes of Health (NIH) Guide for the Care and Use of Laboratory Animals (Ethic No. IR.MUI.RESEARCH.REC.1400.493). A total of twenty-seven Wistar rats, weighing 180-220 g, were randomly divided into three groups, each containing nine animals. The three groups were designated as follows:

Control: no treatment; Gel/HA nanofibers: treatment with Gel/HA nanofibers; Gel/HA nanofibers/Ag NPs/phenytoin: treatment with Gel/HA nanofibers containing Ag NPs and phenytoin.

The drug-loaded Gel/HA nanofibers contained approximately 0.5% w/v Ag NPs and 0.5% w/v phenytoin, ensuring effective localized release at the wound site. To induce anesthesia, the animals were intraperitoneally administered ketamine (75 mg/kg). Once anesthetized, the dorsal skin was shaved to remove hair. The animals were then placed in a prone position on a sterile surgical table, and a full-thickness excisional wound involving both dermis and hypodermis was created. A full-thickness circular excisional wound with a diameter of 1.5 cm was created on the dorsal skin of each rat under aseptic conditions.

The respective treatments were applied to the wounds, then gently blotted dry using sterile gauze. The wounds were not splinted, acknowledging that murine wounds predominantly heal through contraction rather than re-epithelialization. This limitation is discussed in the manuscript to provide context for the observed healing outcomes. The wound healing ratio was assessed by photographing each wound on days 0, 5, 10, and 15. The wound area was measured using ImageJ software, and the percentage of wound closure was calculated using the equation below (43):

$$\text{Wound healing ratio (\%)} = \frac{\text{Initial wound area} - \text{wound area on day X}}{\text{Initial wound area}} \times 100 \quad (5)$$

For histological analysis, wound tissue samples were harvested on days 5, 10, and 15 from each of the three groups. The collected specimens were fixed in 10% formalin and then dehydrated through a graded series of ethanol-xylene solutions. The samples were then paraffin-embedded (40-60%) and sectioned for further processing. Hematoxylin and eosin (H&E) and Masson's trichrome staining techniques were employed for tissue examination. Histological changes were evaluated under an optical microscope (44).

All animal investigations were approved by the Animal Research Ethics Committee of Isfahan University of Medical Science in Iran (Ethical approval ID: 3400908), and performed in line with the National Institute of Health Guide for the Care and Use of Laboratory Animals (NIH Publications No. 80-23 revised 1996). Possible efforts were made to decrease animal numbers and distress.

Statistical analysis

In this study, all data were analyzed using a one-way ANOVA. To assess statistical significance among the groups, the Tukey-Kramer post hoc test was applied using Graph Pad Prism Software (V.9). A P-value < 0.05 was considered statistically significant.

RESULTS

Characterization of Ag NPs

The synthesis and characterization of Ag NPs were validated through morphological and spectral analyses. The SEM images (Fig.1A and B)

illustrate the formation of spherical Ag NPs with uniform morphology. The size measurements in Fig.1B revealed that the average diameter of the synthesized Ag NPs is approximately 40 nm, consistent with the narrow size distribution previously calculated (PDI = 0.35 ± 0.02).

The UV-visible spectroscopy results further corroborate these findings. The absorption spectrum (Fig. 1C) shows a distinct peak at 423 nm, characteristic of the surface plasmon resonance of spherical Ag NPs. The peak position confirms the particle size observed in the SEM images, as the surface plasmon resonance wavelength correlates with the size and shape of metallic nanoparticles. The shift of the absorption peak to a longer wavelength also supports the formation of well-defined, larger nanoparticles, free from significant agglomeration.

Characterization of nanofibers wound dressing

SEM

The morphological analysis of the electrospun Gel/HA nanofibers was carried out using SEM, as illustrated in Fig. 2. The SEM images revealed that all formulations produced smooth, bead-free nanofibers, with uniform morphology across different compositions. As seen in Fig. 3, the average fiber diameter was significantly influenced by the formulation's composition and the presence of a cross-linker. Specifically, the average diameters of the Gel/HA nanofibers were measured at 364.16 ± 55 nm, 488.97 ± 43 nm, and 635.67 ± 68 nm for formulations FG20HA0.15, FG20HA0.25, and FG20HA0.35, respectively. Moreover, incorporating a cross-linker further enhanced the fiber diameter, as evidenced by formulation FG20HA0.25C, which exhibited an average diameter of 597.53 ± 61 nm. The presence of the cross-linker increased the viscosity of the electrospinning solution, leading to thicker fibers than the non-cross-linked formulation FG20HA0.25. Interestingly, the addition of Ag NPs did not result in any significant changes to the fiber morphology or shape, as shown in Figs. 2 and 3.

FTIR

FTIR spectroscopy was employed to confirm the integration of Ag NPs, Gel, HA, and phenytoin within the nanofiber structure, as illustrated in Fig. 4. The spectrum of Gel (Fig. 4A) exhibits characteristic peaks corresponding to the O-H stretch at 3436 cm^{-1}, the C=O stretch at 1642 cm^{-1}, the amide II (N-H bend and C-H stretch) peak at 1542 cm^{-1}, and the amide III (C-N stretch and N-H bend) peak at 1235 cm^{-1}. These peaks are indicative of Gel's functional groups (45).

The HA spectrum (Fig. 4B) demonstrates peaks at 3423 cm^{-1} for the O-H stretch, 1618 cm^{-1} for the C=O stretch, 1413 cm^{-1} for the symmetric -COO stretch, and 1044 cm^{-1} for the ether bond. These peaks represent the characteristic vibrations of HA. The combined Gel and HA nanofiber spectrum (Fig. 4C) shows overlapping peaks, with O-H stretch vibrations at 3289 cm^{-1} and symmetric and asymmetric -COO stretch vibrations at 1535 cm^{-1} and 1448 cm^{-1}, respectively. Additionally, the C=O stretch peak at 1647 cm^{-1} is shifted due to interactions between the NH_2 group of Gel and the carboxylic group of HA, confirming the compatibility of Gel and HA within the nanofiber structure (31).

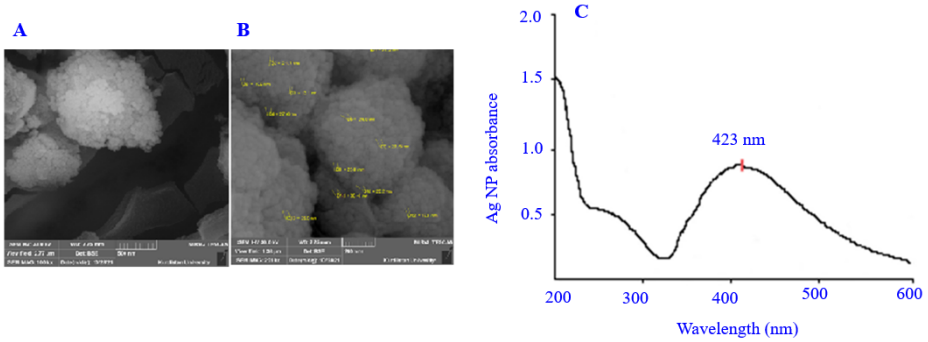

Fig. 1. FE-SEM picture of Ag NPs at magnifications of (A) ×100000 and (B) ×200000, and (C) the UV-visible absorption spectrum of Ag NPs with a concentration of 42.5 µg/mL (λ_{max} = 423 nm). Ag NP, Silver nanoparticle; FE-SEM, field-emission scanning electron microscopy.

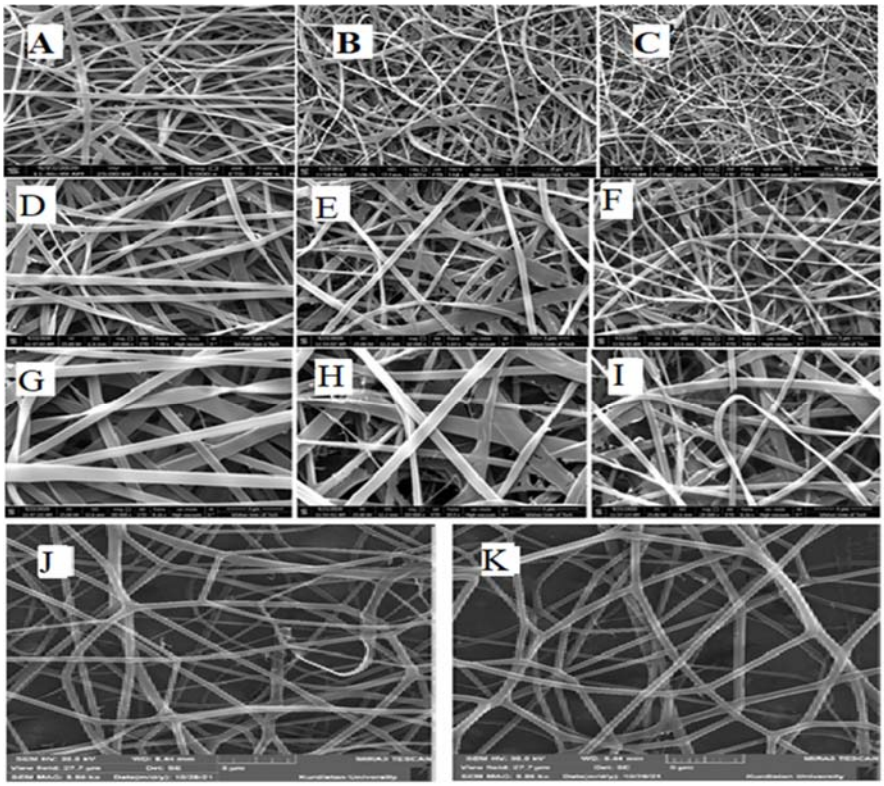

Fig. 2. FE-SEM images of Gel/HA nanofibers at magnifications of 5000, 10,000, and 20,000 in pre-optimal nanofiber formulations FG20HA0.15, FG20HA0.25, and FG20HA0.35. FE-SEM image of nanofibers containing Gel/HA with 5000 magnifications in formulations (A) FG20HA0.15, (B) FG20HA0.25, and (C) FG20HA0.35. FE-SEM image of nanofibers containing Gel/HA with 10000 magnifications in formulations (D) FG20HA0.15, (E) FG20HA0.25, and (F) FG20HA0.35. FE-SEM image of nanofibers containing Gel/HA with 20000 magnifications in formulations (G) FG20HA0.15, (H) FG20HA0.25, and (I) FG20HA0.35. FE-SEM image of nanofibers containing Gel/HA in their (J) optimum formulation (FG20HA0.25), crosslinker (FG20HA0.25C), and (K) drug (FG20HA0.25CD) at a magnification of × 10000. Gel, Gelatin; HA, hyaluronic acid; FE-SEM, field-emission scanning electron microscopy.

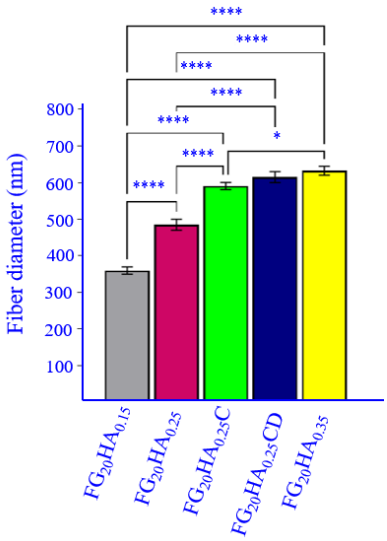

Fig. 3. Fiber diameter of nanofibers in pre-optimized formulations of Gel/HA nanofibers. All values are presented as mean ± SD, n = 3. **P* < 0.05 and *****P* < 0.0001 indicate significant differences between designated groups. Gel, Gelatin; HA, hyaluronic acid.

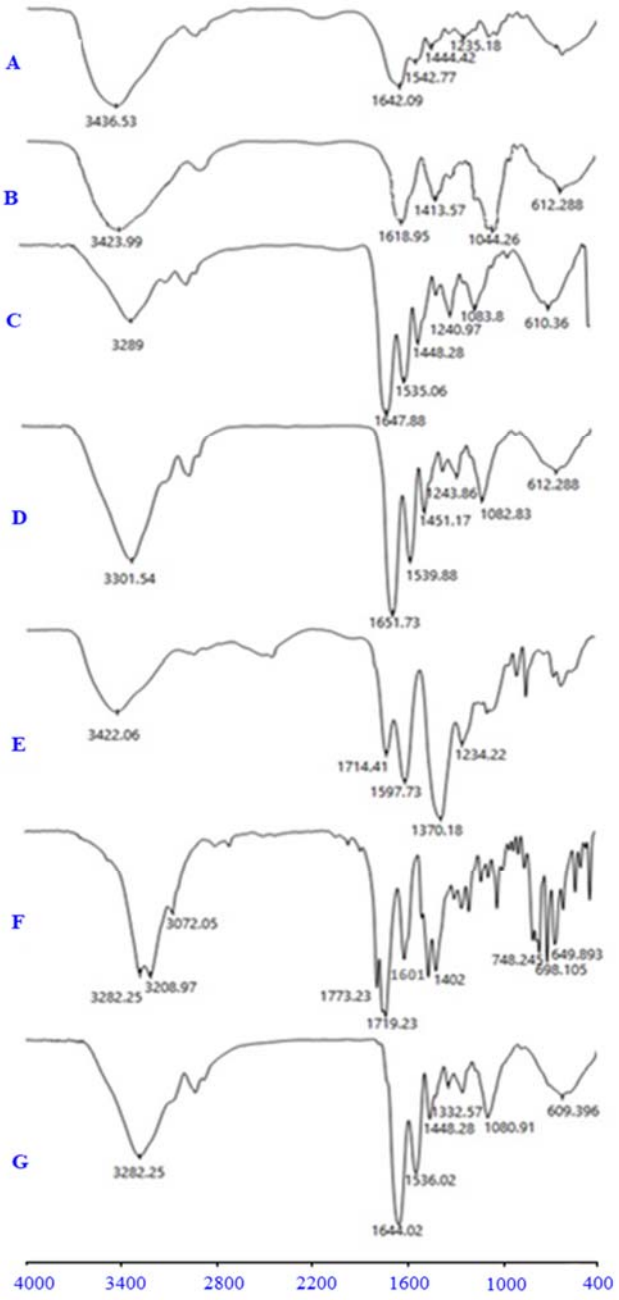

Fig. 4. FTIR spectra of (A) Gel, (B) HA, (C) Gel and HA film, (D) cross-linked film of Gel and HA by glyoxal, (E) Ag NPs, (F) phenytoin, (G) the cross-linked film with glyoxal containing Ag NPs and phenytoin. FTIR, Fourier-transform infrared; Gel, gelatin; HA, hyaluronic acid; Ag NP, silver nanoparticle.

When cross-linked with glyoxal, the Gel/HA nanofiber spectrum (Fig. 4D) reveals a distinct peak at 1451 cm^{-1}, attributed to the formation of aldimine (CH=N) bonds, which result from the interaction between glyoxal's aldehyde group and Gel's amine groups (46). This peak confirms the successful cross-linking of Gel and HA. The Ag NPs spectrum (Fig. 4E) features a prominent peak at 1714 cm^{-1}, corresponding to the C=O stretch, which signifies the oxidation of tannic acid to quinone. Furthermore, peaks at 1597 cm^{-1} and 1370 cm^{-1} are associated with asymmetric and symmetric C=O stretch vibrations of the -COO group, indicating the stabilization of Ag NPs by citrate and tannic acid ions during synthesis (47).

The phenytoin spectrum (Fig. 4F) displays characteristic peaks at 3282 cm^{-1} and 3208 cm^{-1}, corresponding to NH stretch vibrations. Peaks at 1773 cm^{-1} and 1719 cm^{-1} are attributed to the C=O stretch, while the peak at 1601 cm^{-1} represents C=C aromatic bending (48). The spectrum of the cross-linked Gel/HA nanofibers containing Ag NPs and phenytoin (Fig. 4G) shows no additional peaks beyond those observed in the native nanofiber spectra, indicating no significant chemical interactions between Gel, HA, Ag NPs, and phenytoin. This suggests that the incorporation of Ag NPs and phenytoin does not disrupt the structural integrity of the Gel/HA nanofibers.

DSC

The DSC thermograms (Fig. 5A and B) provide insights into the thermal stability of the Gel/HA nanofibers and the effect of incorporating Ag NPs and phenytoin. As shown in Fig. 5B, the composite nanofibers exhibited a noticeable rightward shift in the endothermic peak compared to the plain Gel/HA nanofiber film (Fig. 5A). This shift indicates that the composite nanofibers possess greater thermal stability than the native Gel/HA nanofibers.

XRD

The XRD patterns of Ag NPs, phenytoin, Gel/HA nanofibers, and Gel/HA nanofibers loaded with drugs are presented in Fig. 6. The diffraction peaks at 2Θ = 29°, 38°, 54°, 64°, and 77° in the Ag NPs spectrum (Fig. 6A) confirm their well-defined crystalline structure. Similarly, the phenytoin spectrum (Fig. 6B) shows characteristic peaks at 2Θ = 11°, 16°, 21°, 23°, and 26°, indicating its crystalline nature (49). The Gel/HA nanofibers (Fig. 6C) display a broad amorphous halo, typical of polymeric materials (50). In contrast, the Gel/HA nanofibers loaded with Ag NPs and phenytoin (Fig. 6D) exhibit a weak crystalline peak at 2Θ = 38°, corresponding to Ag NPs. This indicates that Ag NPs are successfully incorporated into the polymer matrix, while phenytoin is likely molecularly dispersed, maintaining the amorphous nature of the nanofibers (51).

Degree of swelling

Figure 7 illustrates the swelling percentages of Gel/HA nanofibers in pre-optimized formulations with and without Ag NPs and phenytoin over a time interval of 2 to 48 h.

The results reveal that the highest swelling percentages were observed for formulations FG20HA0.25C and FG20HA0.35C, with maximum swelling achieved at 24 h. The addition of Ag NPs and phenytoin significantly reduced the swelling capacity of Gel/HA nanofibers compared to those without drugs.

hyaluronic acid; Ag NP, silver nanoparticle.

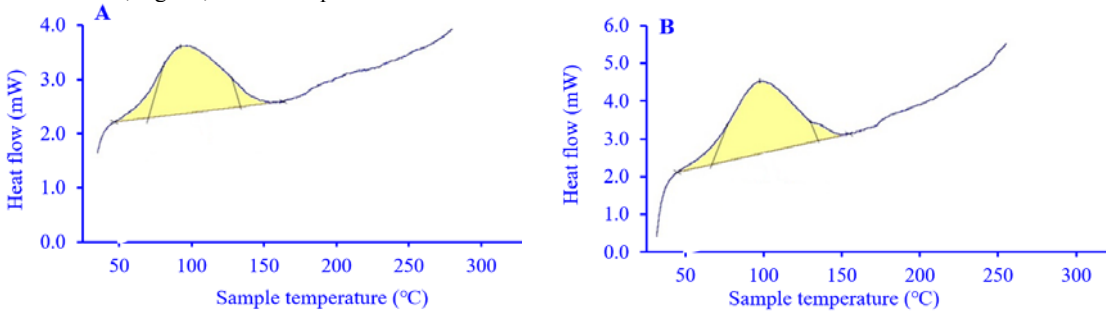

Fig. 5. Differential scanning calorimetry spectra of (A) wound dressing without drugs and (B) wound dressing containing Ag NPs and phenytoin. Ag NP, silver nanoparticle.

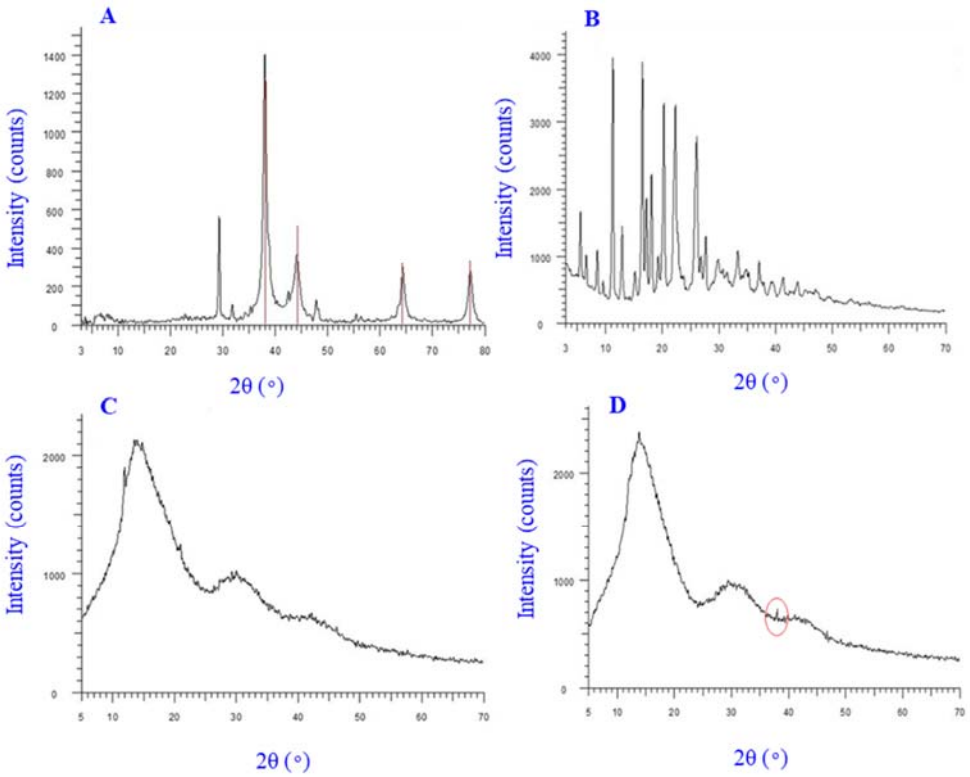

Fig. 6. X-ray powder diffraction spectra of (A) Ag NPs, (B) phenytoin, (C) cross-linked fibers of Gel-HA, (D) Gel-HA cross-linked fibers, and Ag NPs and phenytoin. Gel, Gelatin; HA, hyaluronic acid; Ag NP, silver nanoparticle.

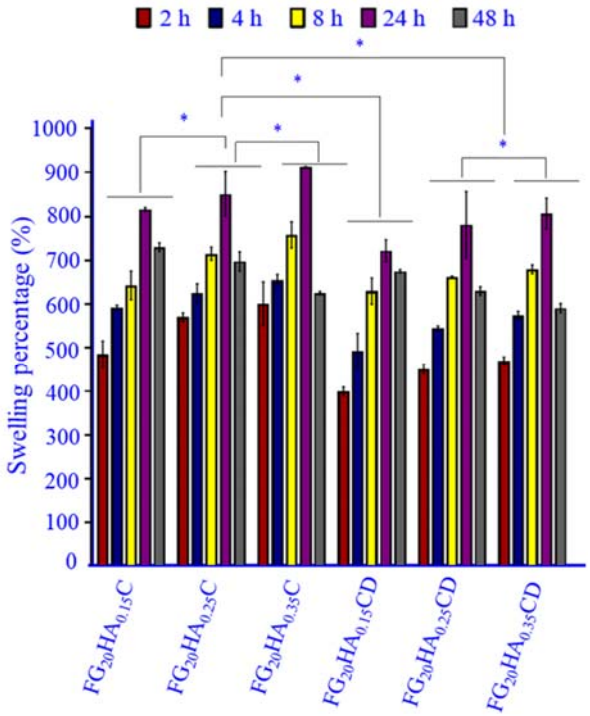

Fig. 7. Swelling percentage of Gel/HA nanofibers in pre-optimal formulations with and without Ag and phenytoin. All values are presented as mean ± SD, n = 3. *$P < 0.05$ indicates significant differences between designated groups. Gel, gelatin; HA, hyaluronic acid; Ag, silver.

Table 1. Results of drug loading percentage in pre-optimal formulations.

Formulation	Gel (g/100 mL)	HA (g/100 mL)	Crosslinker	Phenytoin EE (%)	Ag NPs EE (%)
$FG_{20}HA_{0.15}CD$	20	0.15	+	82.27 ± 2.76*	75.73 ± 2.48*
$FG_{20}HA_{0.25}CD$	20	0.25	+	61.02 ± 2.82$^{\#}$	56.02 ± 1.8$^{\#}$
$FG_{20}HA_{0.35}CD$	20	0.35	+	43.09 ± 3.01	38.06 ± 1.76
$FG_{20}HA_{0.25}D$	20	0.25	+	62.77 ± 2.57$^{\#}$	57.34 ± 1.21$^{\#}$

Gel, Gelatin; HA, hyaluronic acid; EE, entrapment efficacy; Ag NP, silver nanoparticle. *$P < 0.05$ Indicates significant difference greater than other formulations; $^{\#}P < 0.05$ significantly greater than the FG20HA0.35CD formulation.

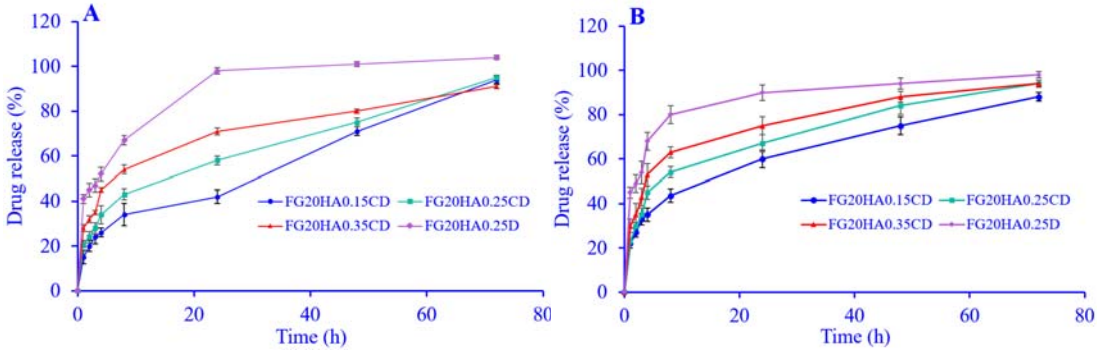

Fig. 8. Release profiles of (A) phenytoin and (B) Ag ion from fabricated composite nanofibers. All values are presented as mean ± SD, n = 3. Ag, Silver.

The entrapment efficiency of Ag NPs and phenytoin

Table 1 provides a summary of the entrapment efficiency of Ag NPs and phenytoin in the synthesized GEL/HA nanofibers and quantifies the amount of drug loaded into the hybrid nanofiber mat. Among the tested formulations, FG20HA0.35CD and FG20HA0.15CD exhibited the lowest and highest drug loadings, respectively. The phenytoin entrapment efficiency ranged from 43.09% to 82.27%, while the Ag NPs entrapment efficiency ranged from 38.06% to 75.73%. Notably, increasing the HA concentration significantly reduced the entrapment efficiency of phenytoin and Ag NPs in the FG20HA0.35CD formulation compared to FG20HA0.25CD and FG20HA0.15CD.

In vitro release studies and release kinetics of Ag NPs and phenytoin

Figure 8 illustrates the release profiles of Ag NPs and phenytoin from the fabricated nanofibers. As illustrated in Fig. 8A, the lowest and highest mean release time (MRT) of phenytoin correspond to formulations FG20HA0.25D and FG20HA0.15CD, with MRTs of 10.22 h and 35.19 h, respectively. The lowest and highest percentages of phenytoin release over 72 h were observed in formulations FG20HA0.35CD and FG20HA0.25D, with release rates of 89.13% and 100%, respectively.

As demonstrated in Fig. 8B, the lowest and highest MRTs of Ag NPs correspond to the formulations FG20HA0.25D and FG20HA0.15CD, with MRTs of 9.67 h and 25.75 h, respectively. The lowest and highest percentages of Ag NP release over 72 h were observed in the formulations FG20HA0.15CD and FG20HA0.25D, with values of 91.46% and 98.54%, respectively.

In vitro antibacterial activity

MICs of Ag NPs against *S. aureus* and *P. aeruginosa* were determined to be 125 µg/mL and 53.125 µg/mL, respectively, demonstrating the exceptional antimicrobial efficacy of Ag NPs. The antimicrobial activity of Ag NPs was further investigated using Gel/HA nanofibers containing Ag NPs and phenytoin, as depicted in Figs. 9-12. Figures 9 and 10 demonstrate the reduction in colony numbers for *S. aureus* and *P. aeruginosa* at nanofiber weights of 4 mg and 5 mg, indicating a significant antibacterial effect. Similarly, Figs. 11 and 12 illustrate the suppression of bacterial growth using the plate well diffusion method, where the nanofibers containing Ag NPs demonstrated effective bacterial inhibition. Notably, Table 2 confirms that incorporating Ag into the nanofibers did not alter its inherent antibacterial properties.

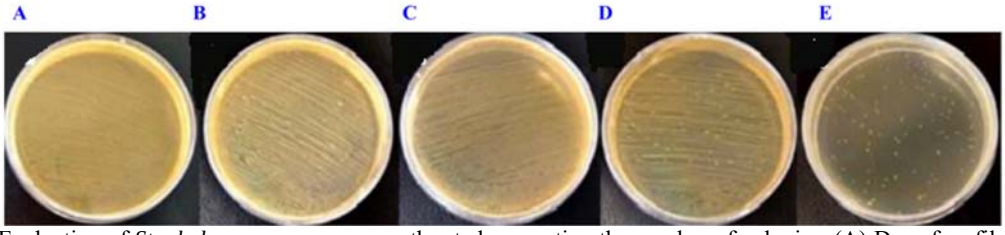

Fig. 9. Evaluation of *Staphylococcus aureus* growth rate by counting the number of colonies. (A) Drug-free film (B-E) different weights of Gel/HA nanofibers containing Ag and phenytoin NPs dissolved in water. Gel, Gelatin; HA, hyaluronic acid; Ag NP, silver nanoparticle.

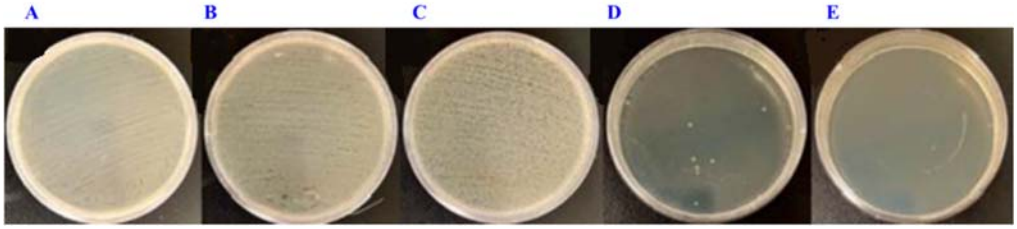

Fig. 10. Count colonies to determine the growth rate of *Pseudomonas aeruginosa*. (A) A drug-free film and (B-E) various weights of Gel/HA nanofibers containing Ag and phenytoin NPs dissolved in water. Gel, Gelatin; HA, hyaluronic acid; Ag NP, silver nanoparticle.

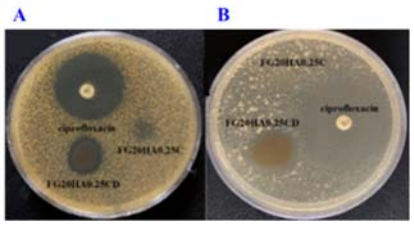

Fig. 11. (A) *Staphylococcus aureus* and (B) *Pseudomonas aeruginosa* growth inhibition halo using the disk diffusion technique with 5 mg Gel/HA nanofibers containing Ag and phenytoin NPs. Gel, Gelatin; HA, hyaluronic acid; Ag NP, silver nanoparticle.

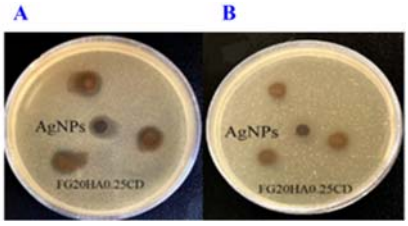

Figure 12. Bacterial growth inhibition halo in the presence of nanofibers containing Ag and phenytoin NPs and Ag NPs against (A) *Staphylococcus aureus* and (B) *Pseudomonas aeruginosa* using the plate well technique. Gel, Gelatin; HA, hyaluronic acid; Ag NP, silver nanoparticle.

Table 2. Antibacterial activity reported as inhibition zone diameter in disc diffusion and plate well method. All values are presented as mean ± SD, n = 3.

Type of sample	Inhibition zone diameter (mm)	
	Staphylococcus aureus	***Pseudomonas aeruginosa***
Gel/HA nanofiber containing drugs in disc diffusion method	8.10 ± 0.74	10.83 ± 0.76
Gel/HA nanofiber in disc diffusion method	0.00	0.00
Gel/HA nanofiber containing drugs in plate well method	7.83 ± 0.19	11.67 ± 0.29
Ag NPs in plate well method	7.67 ± 0.25	11.50 ± 0.50

Gel, Gelatin; HA, hyaluronic acid; Ag NP, silver nanoparticle.

In-vivo evaluation of wound dressing

Figures 13 and 14 depict the physical assessment of wound healing in three experimental groups: the control group, the group treated with drug-free nanofibers, and the group treated with drug-loaded nanofibers. The healing process varied significantly among these groups, with the control group showing the slowest rate of recovery. In contrast, the group treated with drug-loaded nanofibers demonstrated the most accelerated wound healing, characterized by complete epithelial development and enhanced tissue regeneration.

Ten days post-injury, epithelial development and connective tissue formation were evident in both the drug-free and drug-loaded nanofiber groups, while the control group exhibited delayed healing. By day 15, the drug-loaded nanofiber group displayed complete epithelialization, the formation of connective tissue, and the regeneration of blood vessels, hair follicles, and sebaceous glands. These results suggest comprehensive skin regeneration with minimal inflammatory cell infiltration.

In contrast, the control group showed larger wound sizes and lacked the regeneration of connective tissue, blood vessels, sebaceous glands, or hair follicles on days 10 and 15. This lack of regeneration is consistent with findings from similar studies that emphasize the necessity of incorporating active agents like Ag NPs and phenytoin to enhance wound healing outcomes.

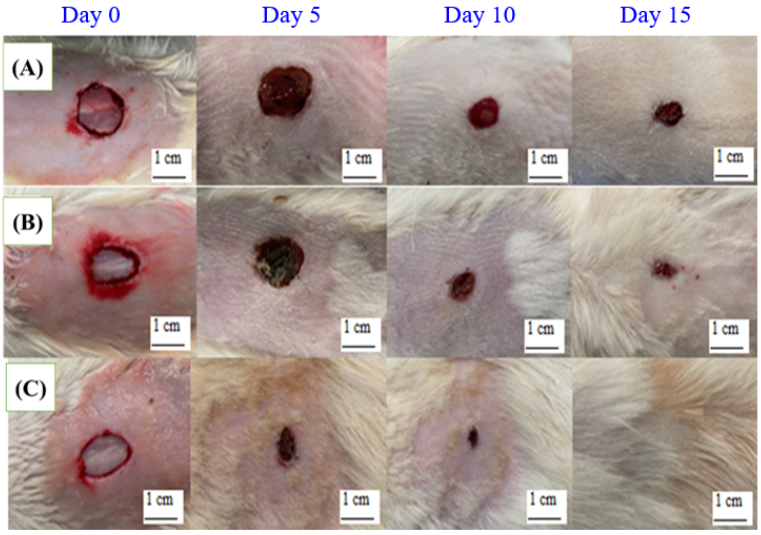

Fig. 13. Evaluation of wound healing in rats at 0, 5, 10, and 15-day intervals; in the (A) control group, (B) nanofibers without drugs, and (C) nanofibers with drugs.

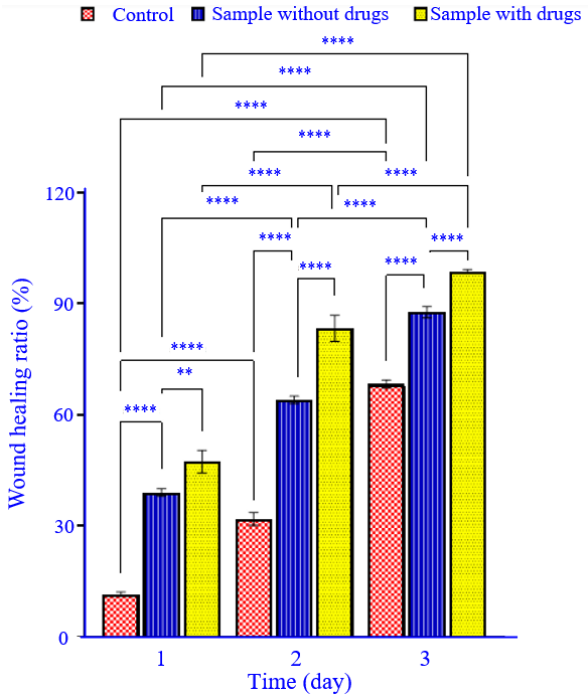

Fig. 14. Quantitative analysis of wound healing ratio (%) during 15 days. All values are presented as mean ± SD, n = 3. $^{**}P < 0.01$ and $^{****}P < 0.0001$ indicate significant differences between designated groups.

Figures 15 and 16 illustrate the histological analysis of wound healing in rats across three experimental groups: the control group, recipients of drug-free nanofibers, and recipients of drug-containing nanofibers. The evaluation was conducted on days 5, 10, and 15 post-injury using hematoxylin-eosin (H&E) and Masson's trichrome staining at 10× magnification, respectively. Figure 15 reveals distinct differences in wound healing progress between the study groups. The control group exhibited the slowest healing rate, with incomplete epithelialization and minimal connective tissue formation observed even by day 15. In contrast, the drug-free nanofiber group demonstrated improved wound healing, with visible epithelial and connective tissue formation by day 10. However, the most pronounced healing was observed in the group receiving drug-loaded nanofibers, which showed complete epithelial regeneration and connective tissue formation by day 15.

Figure 16 provides insights into collagen deposition and tissue remodeling during the healing process. In the control group, minimal collagen deposition was observed throughout the 15-day period, with poorly organized connective tissue. In the drug-free nanofiber group, moderate collagen deposition was evident by day 10, increasing by day 15, though the fibers remained less organized compared to the natural skin structure.

In contrast, the group treated with drug-loaded nanofibers exhibited significantly enhanced collagen deposition. By day 15, compact, dense, and mature collagen fibers were arranged parallel to the epidermis, closely resembling the structure of normal skin. This enhanced collagen organization and deposition contribute to stronger and more functional skin regeneration. Additionally, the wound length in this group was significantly reduced compared to the control and drug-free nanofiber groups, highlighting the effectiveness of the drug-loaded nanofibers in promoting faster and more complete wound closure.

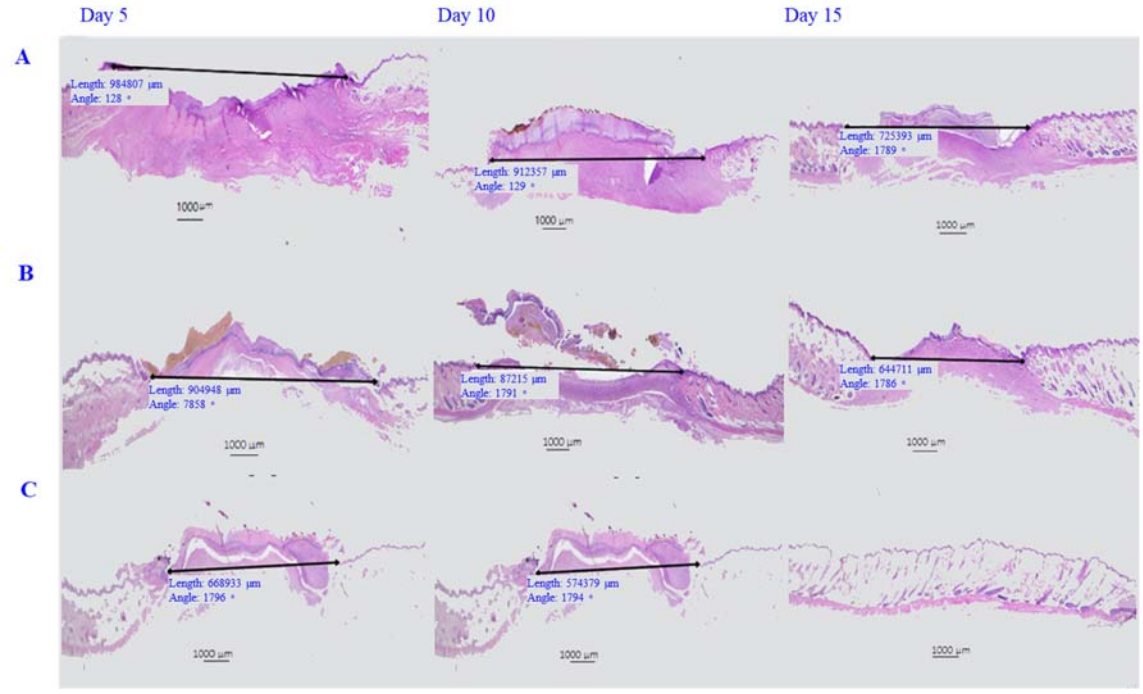

Fig. 15. Staining using hematoxylin-eosin dye with magnification × 10. Histological analysis of rat wound healing on days 5, 10, and 15 in (A) control samples, (B) nanofibers without drugs, and (C) nanofibers with drugs.

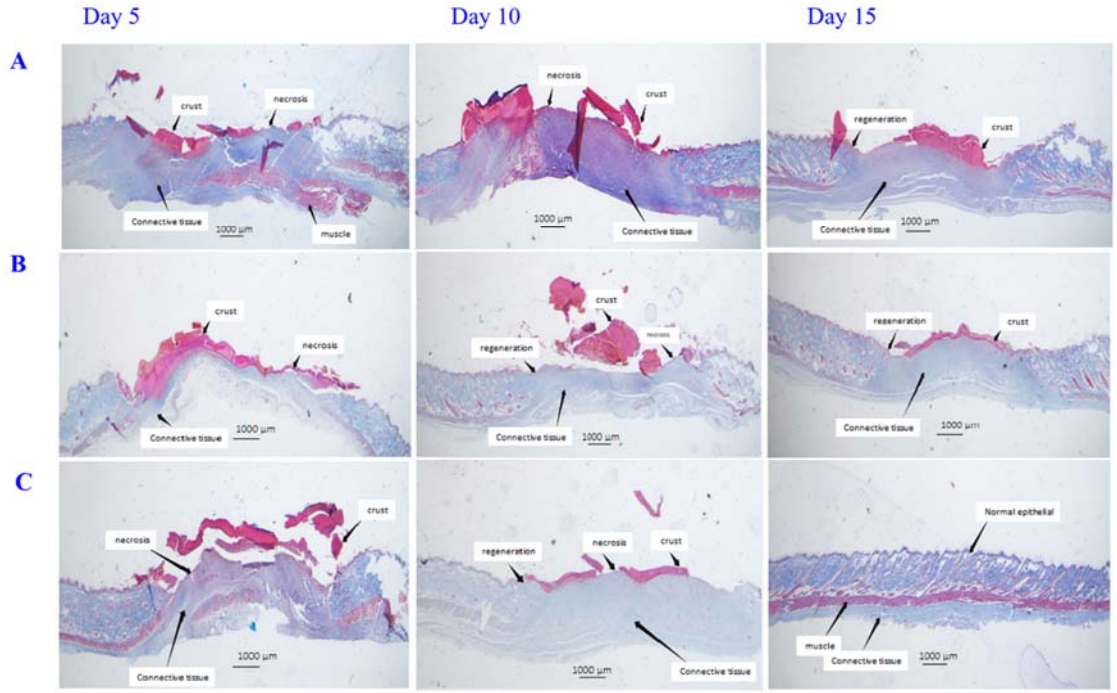

Fig. 16. Staining using trichrome Masson dye with magnification × 10. Histological analysis of rat wound healing on days 5, 10, and 15 in (A) control samples, (B) nanofibers without drugs, and (C) nanofibers with drugs.

DISCUSSION

This uniformity of the synthesized NPs indicates the efficiency of the reduction process facilitated by trisodium citrate and tannic acid. Trisodium citrate not only acted as a reducing agent but also as a stabilizer, forming a compact surface layer, as suggested by the ZP measurement of -23.77 mV, which ensures the colloidal stability of the Ag NPs in aqueous media (52,53).

The role of tannic acid in this synthesis cannot be understated. Its dual function as a reducing and stabilizing agent not only accelerated the formation of Ag NPs but also controlled their size distribution. This is evident from the consistent spherical morphology and narrow size distribution in the SEM images. Additionally, the uniform particle size and compact citrate layer suggest that this synthesis method is highly efficient and suitable for reproducible nanoparticle production (54,55).

Overall, the data confirm the successful synthesis of Ag NPs with excellent morphological and size uniformity, high stability, and reproducibility. These properties make the synthesized Ag NPs suitable for various biomedical and industrial applications, including their integration into Gel/HA nanofibers for antibacterial and wound-healing studies. Future studies could explore optimizing the synthesis parameters to further improve the scalability while maintaining uniformity in particle size and morphology.

The morphological analysis of the electrospun Gel/HA nanofibers revealed that increasing the HA content in the formulations led to a significant increase in fiber diameter, particularly in FG20HA0.35, where the average diameter was 635.67 ± 68 nm. This finding aligns with previous studies, such as those conducted by Lian *et al*. (56), and can be attributed to the increased viscosity of the electrospinning solution with higher HA concentrations. Higher solution viscosity generally results in larger fiber diameters, as the electrospinning process is more resistant to stretching forces. These results underscore the critical role of HA concentration in modulating the physical properties of Gel/HA nanofibers.

The observed enhancement in nanofiber diameter due to the presence of cross-linkers

aligns with recent research. Studies have indicated that cross-linking agents contribute to increased fiber diameter by influencing both solution viscosity and polymer chain interactions (46,57). This suggests that the cross-linkers promote a more robust and interconnected network, ultimately leading to the formation of thicker fibers.

However, the morphology of the fibers loaded with Ag NPs remained stable, which can be attributed to the protective role of Gel, which likely prevented any structural disruption during the incorporation of Ag NPs. The uniform distribution of Ag NPs within the fibers ensures their consistent integration without compromising the nanofibers' structural integrity (58).

Overall, the findings highlight the tunability of Gel/HA nanofiber characteristics by modifying the HA concentration and incorporating cross-linkers. The ability to control fiber diameter and morphology is critical for optimizing nanofiber-based materials for specific biomedical applications, such as wound dressings. Larger fiber diameters, influenced by higher viscosity, may improve the mechanical properties and drug-loading capacity of the fibers, while maintaining smooth and uniform morphology, ensuring consistency in application (59). These results further validate the potential of Gel/HA nanofibers as an adaptable platform for advanced wound-healing materials.

All the peaks corresponding to Ag NPs, along with the peaks related to phenytoin, are visible in the spectrum of the film cross-linked by glyoxal and containing both Ag NPs and phenytoin. Additionally, all characteristic peaks of HA and gelatin were observed in the following films: the Gel/HA film, the glyoxal-cross-linked Gel/HA film, and the glyoxal-cross-linked film containing Ag NPs and phenytoin. This confirms the presence of both polymers in the aforementioned films. By analyzing these spectra, it can be concluded that no molecular interactions occurred that would alter the chemical structure of the drugs. In the spectrum of the glyoxal-cross-linked film containing Ag NPs and phenytoin, the intensity of the peaks is significantly lower compared to the pure drugs due to the low drug content in the samples.

DSC thermogram analysis indicates that composite nanofibers exhibit enhanced thermal stability compared to native Gel/HA nanofibers. This increased thermal stability can be attributed to the electrostatic interactions between Gel and Ag NPs, which enhance the structural integrity of the nanofibers. These interactions prevent the breakdown of the polymer matrix under elevated temperatures. Additionally, the adsorption of Gel onto the surface of Ag NPs due to its protective properties further stabilizes the nanoparticles within the composite nanofiber matrix. This stabilization prevents nanoparticle aggregation and contributes to the improved thermal performance of the composite. Moreover, the semiconductor properties of Ag NPs play a crucial role in enhancing the heat conductivity of the composite nanofibers. This increased heat transfer capability allows the composite structure to dissipate heat more efficiently, further contributing to its thermal stability (60,61).

The XRD findings demonstrate that the incorporation of Ag NPs and phenytoin not only enhances the functional properties of the nanofibers but also improves their thermal robustness, making them suitable for applications requiring sustained performance under various conditions.

These results demonstrate the structural compatibility of Ag NPs and phenytoin with the Gel/HA matrix, ensuring stable integration without disrupting the polymer's flexibility. The crystalline integrity of Ag NPs supports their sustained antimicrobial activity, while the amorphous dispersion of phenytoin likely enhances its bioavailability and controlled release. Together, these findings highlight the potential of Gel/HA nanofibers as multifunctional wound dressings with enhanced thermal stability, antimicrobial activity, and therapeutic efficacy.

The swelling capacity of polymeric nanofibers plays a critical role in controlling the release of therapeutic compounds from the nanofiber matrix (62).

The incorporation of Ag NPs and phenytoin into Gel/HA nanofibers resulted in a notable decrease in swelling capacity relative to drug-free nanofibers. This reduction can be attributed

to several factors, including a higher polymer content in nanofibers without drugs, which allows for greater water uptake, the formation of hydrogen bonds within the polymer network, and the restricted swelling capacity due to the presence of Ag NPs and phenytoin, which may interact with the polymer chains and limit their expansion (63).

These findings are consistent with observations reported by Rath *et al.*, who demonstrated that the swelling behavior of polymer nanofibers is a critical factor influencing the release profile of encapsulated drug molecules (3). The reduced swelling in nanofibers containing Ag NPs and phenytoin indicates improved structural integrity and controlled swelling, which are essential for sustained drug release applications. Overall, the swelling behavior of Gel/HA nanofibers can be modulated by adjusting the formulation parameters, including HA content, cross-linking, and the inclusion of drugs. These results highlight the potential of Gel/HA nanofibers as a versatile platform for drug delivery systems, where controlled swelling is vital for ensuring the sustained release of therapeutic agents.

Increasing the concentration of HA has a demonstrable impact on diminishing the entrapment efficiency of phenytoin and Ag NPs. This reduction can be attributed to the passive loading mechanism employed during the fabrication process. The incorporation of Ag NPs and phenytoin into the polymer nano-matrix during electrospinning appears to have been influenced by the solution's viscosity. As the HA concentration increased, the viscosity of the electrospinning solution also rose, leading to greater loss of the electrospinning fluid. This heightened viscosity likely impeded the efficient incorporation of the drug and nanoparticles into the nanofibers, reducing their overall load (64,65).

In summary, while HA contributes to the viscosity of the electrospinning solution, its excessive addition can negatively impact the drug and nanoparticle entrapment efficiencies (66). This highlights the need for optimizing the HA concentration to balance the viscosity and achieve effective drug and nanoparticle loading within GEL/HA nanofibers. Future investigations should explore additional parameters, such as electrospinning voltage, flow rate, and solvent composition, to enhance the overall drug and nanoparticle loading capacity while maintaining the structural integrity of the nanofibers.

The drug release behavior from the nanofibers is influenced by multiple factors, including surface drug desorption and diffusion through microporous channels, which are formed as a result of the swelling behavior of the nanofiber matrix. The release process begins with the desorption of physically adsorbed drugs from the nanofiber surface, followed by a diffusion-controlled mechanism through these microporous structures (67).

Several factors contribute to the observed release profiles. The initial burst release of drugs may be attributed to the high surface-to-volume ratio of the nanofibers, the presence of micro-porous structures, and electrostatic interactions between Ag NPs and gelatin (68). Despite the large surface area, the formulations exhibited only a slight burst release, which is likely moderated by these electrostatic interactions. Following this initial phase, drug release is predominantly controlled by diffusion through the intact and swollen polymer matrix.

To further understand the drug release mechanism, the release data were analyzed using various mathematical models. The Higuchi model was identified as the most appropriate framework for describing the release mechanism of the Ag NPs and the drug from the nanofibers. This model suggests that the release process is governed by Fickian diffusion, where the drug diffuses through the polymer matrix in response to a concentration gradient. The suitability of this model indicates that the release is primarily controlled by the physical structure of the nanofibers and the gradual movement of the drug through the porous network, providing a sustained and predictable release profile (50). In addition to the Higuchi model, the Korsmeyer-Peppas model was applied to further investigate the release mechanism. The calculated release exponent (n) values ranged from 0.45 to 0.5, confirming that the release follows a predominantly Fickian diffusion mechanism, consistent with the diffusion-controlled profile

suggested by the Higuchi model. Also, the rate of drug diffusion is directly influenced by the degree of water absorption in the Gel/HA matrix. However, cross-linking significantly reduces the rate of drug release by limiting water penetration into the polymer core, thereby slowing polymer swelling and degradation.

Swelling experiments revealed that maximum swelling occurred after 24 h, followed by a slight reduction after 48 h, indicating the onset of polymer degradation. This pattern aligns with the release profiles, where a second increase in drug release was observed around the 48-h mark, likely due to the breakdown of the polymeric structure. This degradation further facilitates the release of entrapped drugs, as evidenced by the extended release over the subsequent 24-h period. In conclusion, the release profiles are a combination of surface desorption, diffusion through microporous channels, and polymeric swelling and degradation (69). The optimized formulations demonstrate a controlled release system influenced by the physicochemical properties of the nanofiber matrix and the degree of cross-linking, making them promising candidates for sustained drug delivery applications.

Ag NPs indicated antimicrobial activity against *S. aureus* and *P. aeruginosa*, which is attributed to multiple mechanisms. First, Ag NPs disrupt bacterial cell wall synthesis by binding to the bacterial cell wall surface, weakening its structural integrity. The peptidoglycan layer in both gram-positive and gram-negative bacteria, composed of N-acetyl glucosamine and N-acetyl muramic acid linked by lysozyme-sensitive bonds, is particularly vulnerable. Ag interacts with the tensile C-O bonds within this structure, triggering oxidative reactions that compromise the cell wall. Second, Ag NPs interfere with protein synthesis, halting the production of essential bacterial proteins. Third, Ag NPs inhibit DNA replication by binding to sulfur and phosphorus groups in DNA due to their high affinity for these elements, thereby impairing cellular replication and viability. Finally, metabolic processes are disrupted, further inhibiting bacterial growth (70,71).

The antibacterial efficacy of the fabricated nanofibers was validated using the disc diffusion and plate well-plate methods. The consistency in inhibition zone diameters between the disc diffusion and plate well methods validates that the antibacterial efficacy of Ag NPs remains intact within the nanofiber matrix. The observed antibacterial properties are highly dependent on the concentration of Ag NPs, with higher concentrations resulting in greater reductions in bacterial colonies. This highlights the potent antimicrobial activity of Ag NPs against both gram-positive and gram-negative bacteria. The differential susceptibility of these bacterial strains is attributed to their cell wall composition. The thinner cell walls of *P. aeruginosa* compared to *S. aureus* facilitate easier penetration of Ag NPs or Ag ions, enabling disruption of metabolic processes and amplifying the antibacterial effect. In conclusion, the Gel/HA nanofibers incorporating Ag NPs exhibit robust antibacterial activity, effectively targeting both *S. aureus* and *P. aeruginosa* (72,73). The combination of Ag NPs and the nanofiber matrix ensures sustained antimicrobial efficacy, making these nanofibers promising candidates for biomedical applications, particularly in combating infections caused by gram-positive and gram-negative bacteria (74). This study underscores the potential of Ag NPs as a versatile and potent antimicrobial agent in advanced therapeutic systems. One limitation of this study is the absence of time-kill kinetics data, which would provide valuable insight into the rate of bacterial eradication by Ag NPs and the composite nanofibers. Future studies should incorporate time-kill assays to comprehensively assess the dynamic antibacterial performance and confirm the suitability of the dressing for rapid wound infection management.

Drug-loaded nanofibers present a significant advantage in wound healing. This superior performance is attributed to the combined antimicrobial properties of Ag NPs, the wound-healing capabilities of phenytoin, and the structural benefits provided by Gel and HA.

Phenytoin has been shown to enhance the expression of platelet-derived growth factor-β in macrophages and monocytes, promoting the

repair and growth of connective tissue. It enhances angiogenesis primarily by upregulating growth factors such as vascular endothelial growth factor and platelet-derived growth factor, which stimulate endothelial cell proliferation and neovascularization at the wound site. It also modulates inflammatory mediators and promotes fibroblast activity, thereby creating a favorable microenvironment for new blood vessel formation. This mechanism accelerates the formation of new connective tissue and blood vessels at the wound site, expediting the healing process (75). Additionally, the astringent and hemostatic properties of Ag NPs contribute to quicker scar formation and minimal scarring by facilitating the deposition of soluble proteins (76,77). The synergistic effects of Ag NPs and phenytoin likely explain the advanced healing observed in the drug-containing nanofiber group.

Also, the rapid healing observed in this group highlights the strong antibacterial properties of Ag NPs, which effectively prevent infection, and the wound-healing capabilities of phenytoin (78).

The incorporation of HA and Gel in the nanofibers also played a significant role in accelerating healing. HA is known for its ability to maintain a moist wound environment and promote cell migration, while Gel provides structural support and enhances cell adhesion (77). These properties synergize with the pharmacological effects of Ag NPs and phenytoin to produce a wound dressing with superior therapeutic efficacy.

Comparing these findings with recent studies, similar results have been observed in the application of Ag NPs-loaded wound dressings, which demonstrated enhanced healing through antibacterial action and tissue regeneration. For example, a study by Khan *et al*. reported that Ag NPs-based polyvinylpyrrolidone (PVP)/ polyvinyl alcohol (PVA) hydrogel promoted collagen deposition and accelerated epithelialization in wound healing models (79).

Among all experimental groups, the drug-loaded nanofiber group achieved the highest collagen deposition levels, followed by the drug-free nanofiber group. This further underscores the importance of incorporating bioactive agents to optimize wound healing. In conclusion, the drug-loaded Gel/HA nanofibers demonstrate significant potential as an advanced wound dressing, capable of promoting rapid and complete tissue regeneration, minimizing scarring, and preventing infections. These findings establish a solid foundation for further clinical evaluation and potential application in wound management therapies.

The superior healing in the drug-loaded nanofiber group can be attributed to the combined effects of Ag NPs and phenytoin. Ag NPs provide strong antibacterial activity, minimizing infection and inflammation, while phenytoin promotes the expression of platelet-derived growth factor-β, accelerating connective tissue and blood vessel formation. These effects synergize with the properties of Gel and HA, which enhance cell adhesion and migration, leading to faster wound closure and tissue remodeling.

It should be noted that rodent wound healing predominantly occurs through contraction rather than re-epithelialization, which may not fully represent the human healing process. Future studies could utilize a splinted wound model to better replicate human tissue regeneration and accurately evaluate the wound dressing's therapeutic potential.

However, the combination of Ag NPs and phenytoin in this study appears to produce superior results due to their complementary mechanisms of action. The drug-free nanofiber group also showed improved healing compared to the control group, underscoring the beneficial properties of Gel and HA even in the absence of active pharmaceutical agents.

In conclusion, the histological analysis confirms that drug-loaded nanofibers significantly enhance wound healing by promoting collagen deposition, reducing wound size, and achieving complete epithelial and connective tissue regeneration. These findings highlight the potential of drug-loaded Gel/HA nanofibers as advanced wound dressings for effective and rapid tissue repair. Future studies should further explore the clinical translation of these findings and evaluate their efficacy in more complex wound models.

Although epithelial regeneration, connective tissue formation, and collagen deposition in

rats' skin treated with drug-loaded nanofibers were remarkably enhanced, it should be noted that rodent wound healing predominantly occurs through contraction rather than re-epithelialization, which may not fully represent the human healing process. Future studies could utilize a splinted wound model to better replicate human tissue regeneration and accurately evaluate the wound dressing's therapeutic potential.

However, the combination of Ag NPs and phenytoin in this study appears to produce superior results due to their complementary mechanisms of action. The drug-free nanofiber group also showed improved healing compared to the control group, underscoring the beneficial properties of Gel and HA even in the absence of active pharmaceutical agents.

In conclusion, the histological analysis confirms that drug-loaded nanofibers significantly enhance wound healing by promoting collagen deposition, reducing wound size, and achieving complete epithelial and connective tissue regeneration. These findings highlight the potential of drug-loaded Gel/HA nanofibers as advanced wound dressings for effective and rapid tissue repair. Future studies should further explore the clinical translation of these findings and evaluate their efficacy in more complex wound models.

CONCLUSION

This study demonstrated the potential of drug-loaded Gel/HA nanofibers containing Ag NPs and phenytoin as advanced wound dressings for accelerating wound healing. The incorporation of Ag NPs and phenytoin significantly enhanced the antimicrobial activity, collagen deposition, epithelial regeneration, and overall wound healing compared to drug-free nanofibers and control groups. The histological and *in vivo* analyses revealed that the drug-loaded nanofibers facilitated faster wound closure, complete epithelialization, and the formation of connective tissue, blood vessels, and sebaceous glands within 15 days, indicating effective tissue regeneration with minimal scarring. The antibacterial properties of Ag NPs, coupled with the wound-healing effects of phenytoin and the structural benefits provided by Gel and HA, synergistically contributed to these outcomes. Key findings of this study include the high antibacterial efficacy of the nanofibers against *S. aureus* and *P. aeruginosa*, the enhanced biocompatibility and tissue-regenerative properties of the drug-loaded nanofibers, and their ability to promote collagen maturation and structural organization in healing tissues. These results highlight the potential of this nanofiber-based system for biomedical applications, particularly in the management of chronic and infected wounds.

Despite these promising results, this study has some limitations. The *in vivo* experiments were conducted on a single wound model in rats, which may not fully capture the complexities of human wound healing. Further preclinical studies involving larger animal models and different wound types are required to validate the findings. Additionally, while the study successfully demonstrated the efficacy of Ag NPs and phenytoin, the long-term effects of their sustained release and potential cytotoxicity need to be thoroughly investigated. Future research should also explore the scalability of the nanofiber fabrication process and its feasibility for clinical applications.

In conclusion, this study provides a strong foundation for the development of multifunctional nanofiber-based wound dressings. By addressing the current limitations and expanding the scope of research, these findings can pave the way for translating this technology into clinical practice, offering an effective solution for wound management and tissue regeneration.

Acknowledgments

This study is based on the Pharm.D. thesis (No. 3400908) submitted by N. Mostolizadeh, with financial support from the Research Department of Isfahan University of Medical Sciences, Isfahan, Iran. The Research Vice Chancellery of Isfahan University of Medical Sciences provided additional funding for the project (Grant No. 297144).

Conflict of interest statement

The authors declared no conflict of interest in this study.

Authors' contributions

J. Emami conceived, designed, and supervised the project, reviewed and edited the study protocol, and revised the manuscript; N. Mostolizadeh carried out the experiments and wrote the manuscript; P. Heydari reviewed and edited the manuscript; M. Tabbakhian supervised and participated in the management of the study; A. Zargar Kharazi supervised the preparation of the nanofibers; M. Minaeiyan contributed to *in vivo* studies; F. Hasanzadeh helped in the preparation of the nanoparticles; M. Mirian conducted the antimicrobial evaluation of the study; A. Talebi performed the pathological assessment. The finalized article was read and approved by all authors.

REFERENCES

1. Wiwatwongwana F, Surin P. *In vitro* degradation of gelatin/carboxymethylcellulose scaffolds for skin tissue regeneration. Chem Eng Trans. 2019;74:1555-1560. DOI: 10.3303/CET1974260.
2. You C, Li Q, Wang X, Wu P, Ho JK, Jin R, *et al*. Silver nanoparticle loaded collagen/chitosan scaffolds promote wound healing via regulating fibroblast migration and macrophage activation. Sci Rep. 2017;7(1):10489,1-11. DOI: 10.1038/s41598-017-10481-0.
3. Rath G, Hussain T, Chauhan G, Garg T, Goyal AK. Collagen nanofiber containing silver nanoparticles for improved wound-healing applications. J Drug Target. 2016;24(6):520-529. DOI: 10.3109/1061186X.2015.1095922.
4. Al-Musawi MH, Turki SH, Al-Naymi HAS, Al-salman SS, Boroujeni VV, Alizadeh M, *et al*. Localized delivery of healing stimulator medicines for enhanced wound Treatment. J Drug Deliv Sci Technol. 2024;101(Part A):106212. DOI: 10.1016/j.jddst.2024.106212.
5. Gaspar-Pintiliescu A, Stanciuc AM, Craciunescu O. Natural composite dressings based on collagen, gelatin and plant bioactive compounds for wound healing: a review. Int J Biol Macromol. 2019;138:854-865. DOI: 10.1016/j.ijbiomac.2019.07.155.
6. Heydari P, Varshosaz J, Kharaziha M, Haghjooy Javanmard S. Antibacterial and pH-sensitive methacrylate poly-L-Arginine/poly (β-amino ester) polymer for soft tissue engineering. J Mater Sci Mater Med. 2023;34(4):16,1-15. DOI: 10.1007/s10856-023-06720-8.
7. Shafizadeh S, Heydari P, Zargar Kharazi A, Shariati L. Coaxial electrospun PGS/PCL and PGS/PGS-PCL nanofibrous membrane containing platelet-rich plasma for skin tissue engineering. J Biomater Sci Polym Ed. 2024;35(4):482-500. DOI: 10.1080/09205063.2023.2299073.
8. Huang TY, Wang GS, Tseng CC, Su WT. Epidermal cells differentiated from stem cells from human exfoliated deciduous teeth and seeded onto polyvinyl alcohol/silk fibroin nanofiber dressings accelerate wound repair. Mater Sci Eng C Mater Biol Appl. 2019;104:109986,1-11. DOI: 10.1016/j.msec.2019.109986.
9. Abid S, Hussain T, Nazir A, Zahir A, Ramakrishna S, Hameed M, *et. al*. Enhanced antibacterial activity of PEO-chitosan nanofibers with potential application in burn infection management. Int J Biol Macromol. 2019;135:1222-1236. DOI: 10.1016/j.ijbiomac.2019.06.022.
10. Gruppuso M, Iorio F, Turco G, Marsich E, Porrelli D. Hyaluronic acid/lactose-modified chitosan electrospun wound dressings-crosslinking and stability criticalities. Carbohydr Polym. 2022;288:119375. DOI: 10.1016/j.carbpol.2022.119375.
11. Li S, Dong Q, Peng X, Chen Y, Yang H, Xu W, *et al*. Self-healing hyaluronic acid nanocomposite hydrogels with platelet-rich plasma impregnated for skin regeneration. ACS Nano. 2022;16(7):11346-11359. DOI: 10.1021/acsnano.2c05069.
12. Su S, Bedir T, Kalkandelen C, Başar AO, Şaşmazel HT, Ustundag CB, *et al*. Coaxial and emulsion electrospinning of extracted hyaluronic acid and keratin-based nanofibers for wound healing applications. Eur Polym J. 2021;142: 110158. DOI: 10.1016/j.eurpolymj.2020.110158
13. Paladini F, Pollini M. Antimicrobial silver nanoparticles for wound healing application: progress and future trends. Materials (Basel). 2019;12(16):2540,1-16. DOI: 10.3390/ma12162540.
14. Echavarría JO, Vanegas NAG, Orozco CPO. Chitosan/carboxymethyl cellulose wound dressings supplemented with biologically synthesized silver nanoparticles from the ligninolytic fungus Anamorphous *Bjerkandera* sp. R1. Heliyon. 2022;8(9):e10258,1-11. DOI: 10.1016/j.heliyon.2022.e10258.
15. Ye H, Cheng J, Yu K. *In situ* reduction of silver nanoparticles by gelatin to obtain porous silver nanoparticle/chitosan composites with enhanced antimicrobial and wound-healing activity. Int J Biol Macromol. 2019;121:633-642. DOI: 10.1016/j.ijbiomac.2018.10.056.
16. Fatima M, Hanif S, Elsharkawy ER, Zafar F, Zulfiqar A, Khan MA, *et al*. Design and fabrication of machine learning trained silver nanoparticles-infused multi-walled carbon nanotube-based sensor for antiviral drug monitoring. Microchem J. 2024;203:110921. DOI: 10.1016/j.microc.2024.110921.
17. Li C, Liu Z, Liu S, Tiwari SK, Thummavichai K, Ola O, *et al*. Antibacterial properties and drug release study of cellulose acetate nanofibers containing ear-like Ag-NPs and Dimethyloxallyl Glycine/beta-cyclodextrin. Appl Surf Sci. 2022;590:153132. DOI: 10.1016/j.apsusc.2022.153132.

18. Ovais M, Ahmad I, Khalil AT, Mukherjee S, Javed R, Ayaz M, *et al*. Wound healing applications of biogenic colloidal silver and gold nanoparticles: recent trends and future prospects. Appl Microbiol Biotechnol. 2018;102(10):4305-4318. DOI: 10.1007/s00253-018-8939-z.
19. Samadi A, Azandeh S, Orazizadeh M, Bayati V, Rafienia M, Karami MA. Fabrication and characterisation of chitosan/polyvinyl alcohol-based transparent hydrogel films loaded with silver nanoparticles and sildenafil citrate for wound dressing applications. Mater Technol (N Y N Y). 2022;37(5):355-365. DOI: 10.1080/10667857.2020.1842151
20. Nqakala ZB, Sibuyi NRS, Fadaka AO, Meyer M, Onani MO, Madiehe AM. Advances in nanotechnology towards development of silver nanoparticle-based wound-healing agents. Int J Mol Sci. 2021;22(20):11272,1-26. DOI: 10.3390/ijms222011272.
21. Ahire JH, Wang Q, Rowley G, Chambrier I, Crack JC, Bao Y, *et al*. Polyurethane infused with heparin capped silver nanoparticles dressing for wound healing application: synthesis, characterization and antimicrobial studies. Int J Biol Macromol. 2024;282 (Pt 1):136557,1-14. DOI: 10.1016/j.ijbiomac.2024.136557.
22. Qadirifard MS, Qadirifard M, Tavakoli G, Mojeni FA, Mohagheghi SZ, Rafiei SKS, *et al*. Topical phenytoin for wound healing: a narrative review. Wound Pract Res. 2024;32(2):66-78. DOI: 10.33235/wpr.32.2.66-78.
23. Syed Ibrahim AM, Ramakrishnan R, Yasar M. A study of efficacy of topical phenytoin in the management of diabetic ulcer. IOSR J Dent Med Sci. 2017;16(8 Ver. VII):5-11. DOI: 10.9790/0853-1608070511.
24. Heydari P, Varshosaz J, Zargar Kharazi A, Karbasi S. Preparation and evaluation of poly glycerol sebacate/poly hydroxy butyrate core-shell electrospun nanofibers with sequentially release of ciprofloxacin and simvastatin in wound dressings. Polym Adv Technol. 2018;29(6): 1795-1803. DOI:10.1002/pat.4286.
25. Heydari P, Zargar Kharazi A, Asgary S, Parham S. Comparing the wound healing effect of a controlled release wound dressing containing curcumin/ciprofloxacin and simvastatin/ciprofloxacin in a rat model: a preclinical study. J Biomed Mater Res A. 2022;110(2):341-352. DOI: 10.1002/jbm.a.37292.
26. Zhong SP, Zhang YZ, Lim CT. Tissue scaffolds for skin wound healing and dermal reconstruction. Wiley Interdiscip Rev Nanomed Nanobiotechnol. 2010;2(5):510-525. DOI: 10.1002/wnan.100.
27. Meng Q, Li Y, Wang Q, Wang Y, Li K, Chen S, *et al*. Recent advances of electrospun nanofiber-enhanced hydrogel composite scaffolds in tissue engineering. J Manuf Process. 2024;123:112-127. DOI:10.1016/j.jmapro.2024.05.085.
28. Wang Q, Zhang S, Jiang J, Chen S, Ramakrishna S, Zhao W, *et al*. Electrospun radially oriented berberine-PHBV nanofiber dressing patches for accelerating diabetic wound healing. Regen Biomater. 2024;11:rbae063,1-15. DOI: 10.1093/rb/rbae063.
29. Pris M. Influence of different parameters on wet synthesis of silver nanoparticles. Bachelor Thesis. University of Twente. 2014.
30. Rapuntean S, Balint R, Paltinean GA, Tomoaia G, Mocanu A, Racz CP, *et al*. Antibacterial activity of silver nanoparticles obtained by co-reduction with sodium citrate and tannic acid. Studia UBB Chemia. 2018:73-85. DOI: 10.24193/subbchem.2018.3.06.
31. Ebrahimi-Hosseinzadeh B, Pedram M, Hatamian-Zarmi A, Salahshour-Kordestani S, Rasti M, Mokhtari-Hosseini ZB, *et al*. *In vivo* evaluation of gelatin/hyaluronic acid nanofiber as Burn-wound healing and its comparison with ChitoHeal gel. Fibers Polym. 2016;17:820-826. DOI: 10.1007/s12221-016-6259-4.
32. Angarano M, Schulz S, Fabritius M, Vogt R, Steinberg T, Tomakidi P, *et al*. Layered gradient nonwovens of i*n situ* crosslinked electrospun collagenous nanofibers used as modular scaffold systems for soft tissue regeneration. Adv Funct Mater. 2013;23:3277-3285. DOI: 10.1002/adfm.201202816.
33. Anzar S, Hanif S, Shaaban IA, Raza A, Khan MA, Naz A, *et al*. Development of metal oxide nanocomposite-coated electrospun nanofibers for highly sensitive xanthine monitoring. Microchem J. 2024;207:112001. DOI: 10.1016/j.microc.2024.112001.
34. Zargar Kharazi A, Ghebleh A, Shariati L. Fabrication of a tri-layer scaffold with dual release of heparin and PRP for tissue engineering of small-diameter blood vessels. Int J Polym Mater Polym Biomater. 2024;73:1374-1385. DOI: 10.1080/00914037.2023.2289537.
35 Azadani RN, Karbasi S, Poursamar A. Chitosan/MWCNTs nanocomposite coating on 3D printed scaffold of poly 3-hydroxybutyrate/magnetic mesoporous bioactive glass: A new approach for bone regeneration. Int J Biol Macromol. 2024;260(Pt 1):129407. DOI: 10.1016/j.ijbiomac.2024.129407.
36. Zienkiewicz-Strzałka M, Deryło-Marczewska A, Skorik YA, Petrova VA, Choma A, Komaniecka I. Silver nanoparticles on chitosan/silica nanofibers: characterization and antibacterial activity. Int J Mol Sci. 2019;21(1):166. DOI: 10.3390/ijms21010166.
37. Nair SC, Vinayan KP, Mangalathillam S. Nose to brain delivery of phenytoin sodium loaded nano lipid carriers: formulation, drug release, permeation and *in vivo* pharmacokinetic studies. Pharmaceutics.. 2021;13(10):1640. DOI: 10.3390/pharmaceutics13101640.
38. Hosseini SMR, Heydari P, Namnabat M, Azadani RN, Gharibdousti FA, Rizi EM, *et al*. Carboxymethyl

cellulose/sodium alginate hydrogel with anti-inflammatory capabilities for accelerated wound healing; *in vitro* and *in vivo* study. Eur J Pharmacol. 2024;176671.
DOI: 10.1016/j.ejphar.2024.176671.

39. Allend SO, Garcia MO, da Cunha KF, de Albernaz DTF, da Silva ME, Ishikame RY, et al. Biogenic silver nanoparticle (Bio-AgNP) has an antibacterial effect against carbapenem-resistant acinetobacter baumannii with synergism and additivity when combined with polymyxin B. J Appl Microbiol. 2022;132(2):1036-1047.
DOI: 10.1111/jam.15297
40. Dubey P, Bhushan B, Sachdev A, Matai I, Uday Kumar S, Gopinath P. Silver-nanoparticle-incorporated composite nanofibers for potential wound-dressing applications. J Appl Polym Sci. 2015;132:42473,1-12.
DOI: 10.1002/app.42473.
41. Almajhdi FN, Fouad H, Khalil KA, Awad HM, Mohamed SHS, Elsarnagawy T, *et al*. *In-vitro* anticancer and antimicrobial activities of PLGA/silver nanofiber composites prepared by electrospinning. J Mater Sci Mater Med. 2014;25:1045-1053.
DOI: 10.1007/s10856-013-5131-y.
42. Jayaramudu T, Raghavendra GM, Varaprasad K, Reddy GVS, Reddy AB, Sudhakar K, *et al*. Preparation and characterization of poly (ethylene glycol) stabilized nano silver particles by a mechanochemical assisted ball mill process. J Appl Polym Sci. 2016;133:43027,1-8.
DOI: 10.1002/APP.43027.
43. Ehterami A, Salehi M, Farzamfar S, Vaez A, Samadian H, Sahrapeyma S, *et al*. *In vitro* and *in vivo* study of PCL/COLL wound dressing loaded with insulin-chitosan nanoparticles on cutaneous wound healing in rats model. Int J Biol Macromol. 2018;117:601-609.
DOI: 10.1016/j.ijbiomac.2018.05.184.
44. National Institutes of Health. Public health service policy on humane care and use of laboratory animals. Maryland National Institutes Heal Bethesda. 2015,1-28.
Available at: https://olaw.nih.gov/sites/default/files/PHSPolicyLabAnimals.pdf.
45. Derkach SR, Voron'ko NG, Sokolan NI, Kolotova DS, Kuchina YA. Interactions between gelatin and sodium alginate: UV and FTIR studies. J Dispers Sci Technol. 2020;41(5):690-698.
DOI: 10.1080/01932691.2019.1611437.
46. Nguyen TH, Lee BT. Fabrication and characterization of cross-linked gelatin electro-spun nano-fibers. J Biomed Sci Eng. 2010;3:1117,1-8.
DOI: 10.4236/jbise.2010.312145.
47. Ranoszek-Soliwoda K, Tomaszewska E, Socha E, Krzyczmonik P, Ignaczak A, Orlowski P, *et al*. The role of tannic acid and sodium citrate in the synthesis of silver nanoparticles. J Nanopart Res. 2017;19:273,1-15.
DOI: 10.1007/s11051-017-3973-9.
48. Dharani S, Rahman Z, Ali SFB, Afrooz H, Khan MA. Quantitative estimation of phenytoin sodium disproportionation in the formulations using vibration spectroscopies and multivariate methodologies. Int J Pharm. 2018;539(1-2):65-74.
DOI: 10.1016/j.ijpharm.2018.01.005.
49. Singh V, Shrivastava A, Wahi N. Biosynthesis of silver nanoparticles by plants' crude extracts and their characterization using UV, XRD, TEM and EDX. African J Biotechnol. 2015;14(33):2554-2567.
DOI: 10.5897/AJB2015.14692.
50. Alemdar N. Fabrication of a novel bone ash-reinforced gelatin/alginate/hyaluronic acid composite film for controlled drug delivery. Carbohydr Polym. 2016;151:1019-1026.
DOI: 10.1016/j.carbpol.2016.06.033.
51. Lee SJ, Heo DN, Moon JH, Ko WK, Lee JB, Bae MS, *et al*. Electrospun chitosan nanofibers with controlled levels of silver nanoparticles. Preparation, characterization and antibacterial activity. Carbohydr Polym. 2014;111:530-537.
DOI: 10.1016/j.carbpol.2014.04.026.
52. Naganthran A, Verasoundarapandian G, Khalid FE, Masarudin MJ, Zulkharnain A, Nawawi NM, *et al*. Synthesis, characterization and biomedical application of silver nanoparticles. Materials (Basel). 2022;15:427,1-43.
DOI: 10.3390/ma15020427.
53. Mustapha T, Misni N, Ithnin NR, Daskum AM, Unyah NZ. A review on plants and microorganisms mediated synthesis of silver nanoparticles, role of plant metabolites and applications. Int J Environ Res Public Health. 2022;19(2):674,1-17.
DOI: 10.3390/ijerph19020674.
54. Gangwar C, Yaseen B, Kumar I, Singh NK, Naik RM. Growth kinetic study of tannic acid mediated monodispersed silver nanoparticles synthesized by chemical reduction method and its characterization. ACS Omega. 2021;6(34):22344-22356.
DOI: 10.1021/acsomega.1c03100.
55. Gangwar C, Yaseen B, Nayak R, Praveen S, Singh NK, Sarkar J, *et al*. Silver nanoparticles fabricated by tannic acid for their antimicrobial and anticancerous activity. Inorg Chem Commun. 2022;141:109532.
DOI: 10.1016/j.inoche.2022.109532.
56. Lian Y, Yuan L, Ji L, Zhang K. Gelatin/hyaluronic acid nanofibrous scaffolds: biomimetics of extracellular matrix. Acta Biochim Biophys Sin. 2013;45:700-703.
DOI: 10.1093/abbs/gmt032.
57. Çallioğlu FC. The effect of glyoxal cross-linker and NaCl salt addition on the roller electrospinning of poly (vinyl alcohol) nanofibers. Tekstil ve Konfeksiyon. 2014;24:15-20.
58. Lu Z, Xiao J, Wang Y, Meng M. *In situ* synthesis of silver nanoparticles uniformly distributed on polydopamine-coated silk fibers for antibacterial application. J Colloid Interface Sci. 2015;452:8-14.
DOI: 10.1016/j.jcis.2015.04.015.
59. Tayebi-Khorrami V, Rahmanian-Devin P, Fadaei MR, Movaffagh J, Askari VR. Advanced applications of smart electrospun nanofibers in cancer therapy:

With insight into material capabilities and electrospinning parameters. Int J Pharm X. 2024;8:100265.
DOI: 10.1016/j.ijpx.2024.100265.
60. Cardoso VS, Quelemes PV, Amorin A, Primo FL, Gobo GG, Tedesco AC, *et al*. Collagen-based silver nanoparticles for biological applications: synthesis and characterization. J Nanobiotechnology. 2014:12:36.
DOI: 10.1186/s12951-014-0036-6.
61. R. Nirmala, K.S. Jeon, R. Navamathavan, M. Park, H.Y. Kim, S.-J. Park, Enhanced electrical properties of electrospun nylon66 nanofibers containing carbon nanotube fillers and Ag nanoparticles. Fibers Polym. 2014;15(5):918-923.
DOI: 10.1007/s12221-014-0918-0.
62. Dong R, Guo B. Smart wound dressings for wound healing. Nano Today. 2021;41:101290.
DOI: 10.1016/j.nantod.2021.101290.
63. Rybka M, Mazurek L, Konop M. Beneficial effect of wound dressings containing silver and silver nanoparticles in wound healing-from experimental studies to clinical practice. Life (Basel). 2022;13(1):69,1-20.
DOI: 10.3390/life13010069.
64. Bhattarai RS, Bachu RD, Boddu SHS, Bhaduri S. Biomedical applications of electrospun nanofibers: drug and nanoparticle delivery. Pharmaceutics. 2018;11(1):5,1-30.
DOI: 10.3390/pharmaceutics11010005.
65. Dodero A, Alberti S, Gaggero G, Ferretti M, Botter R, Vicini S, Castellano M. An up-to-date review on alginate nanoparticles and nanofibers for biomedical and pharmaceutical applications. Adv Mater Interfaces. 2021;8:2100809,1-27.
DOI: 10.1002/admi.202100809.
66. Casey-Power S, Ryan R, Behl G, McLoughlin P, Byrne ME, Fitzhenry L. Hyaluronic acid: its versatile use in ocular drug delivery with a specific focus on hyaluronic acid-based polyelectrolyte complexes. Pharmaceutics. 2022;14(7):1479,1-40.
DOI: 10.3390/pharmaceutics14071479.
67. Gutschmidt D, Hazra RS, Zhou X, Xu X, Sabzi M, Jiang L. Electrospun, sepiolite-loaded poly (vinyl alcohol)/soy protein isolate nanofibers: Preparation, characterization, and their drug release behavior. Int J Pharm. 2021;594:120172.
DOI: 10.1016/j.ijpharm.2020.120172.
68. Herdiana Y, Wathoni N, Shamsuddin S, Muchtaridi M. Drug release study of the chitosan-based nanoparticles. Heliyon. 2022;8(1):e08674,1-16.
DOI: 10.1016/j.heliyon.2021.e08674.
69. Mojahedi M, Heydari P, Kharazi AZ. Preparation and characterization of an antibacterial CMC/PCL hydrogel films containing CIP/Cur: *in vitro* and *in vivo* evaluation of wound healing activity. Int J Biol Macromol. 2024;282(Pt 1):136570.
DOI: 10.1016/j.ijbiomac.2024.136570.
70. Wang L, Liu L, Liu Y, Wang F, Zhou X. Antimicrobial performance of novel glutathione-conjugated silver nanoclusters (GSH@ AgNCs) against *Escherichia coli* and *Staphylococcus aureus* by membrane-damage and biofilm-inhibition mechanisms. Food Res Int. 2022;160:111680.
DOI: 10.1016/j.foodres.2022.111680.
71. Singh M, Mallick AK, Banerjee M, Kumar R. Loss of outer membrane integrity in Gram-negative bacteria by silver nanoparticles loaded with *Camellia sinensis* leaf phytochemicals: plausible mechanism of bacterial cell disintegration. Bull Mater Sci. 2016;39(7):1871-1878.
DOI: 10.1007/s12034-016-1317-5.
72. Ghaseminezhad SM, Shojaosadati SA, Meyer RL. Ag/Fe3O4 nanocomposites penetrate and eradicate *S. aureus* biofilm in an *in vitro* chronic wound model. Colloids Surf B Biointerfaces. 2018;163:192-200.
DOI: 10.1016/j.colsurfb.2017.12.035
73. Ahmed B, Hashmi A, Khan MS, Musarrat J. ROS mediated destruction of cell membrane, growth and biofilms of human bacterial pathogens by stable metallic AgNPs functionalized from bell pepper extract and quercetin. Adv Powder Technol. 2018;29(7):1601-1616.
DOI: 10.1016/j.apt.2018.03.025.
74. Durairaj S, Sridhar D, Ströhle G, Li H, Chen A. Bactericidal effect and cytotoxicity of graphene oxide/silver nanocomposites. ACS Appl Mater Interfaces. 2024;16(15):18300-18310.
DOI: 10.1021/acsami.3c15798.
75. Fattahi N, Abdolahi A, Vahabzadeh Z, Nikkhoo B, Manoochehri F, Goudarzzadeh S, *et al*. Topical phenytoin administration accelerates the healing of acetic acid-induced colitis in rats: evaluation of transforming growth factor-beta, platelet-derived growth factor, and vascular endothelial growth factor. Inflammopharmacology. 2022;30(1):283-290.
DOI: 10.1007/s10787-021-00885-w.
76. Zhang Y, Kang J, Chen X, Zhang W, Zhang X, Yu W, *et al.* Ag nanocomposite hydrogels with immune and regenerative microenvironment regulation promote scarless healing of infected wounds. J Nanobiotechnology. 2023;21(1):435,1-17.
DOI: 10.1186/s12951-023-02209-2.
77. El-Aassar MR, Ibrahim OM, Fouda MMG, El-Beheri NG, Agwa MM. Wound healing of nanofiber comprising polygalacturonic/hyaluronic acid embedded silver nanoparticles: *in-vitro* and *in-vivo* studies. Carbohydr Polym. 2020;238:116175,1-11.
DOI: 10.1016/j.carbpol.2020.116175.
78. Hussein MAM, Guler E, Rayaman E, Cam ME, Sahin A, Grinholc M, *et al*. Dual-drug delivery of Ag-chitosan nanoparticles and phenytoin *via* core-shell PVA/PCL electrospun nanofibers. Carbohydr Polym. 2021;270:118373.
DOI: 10.1016/j.carbpol.2021.118373.
79. Khan MI, Paul P, Behera SK, Jena B, Tripathy SK, Lundborg CS, *et al*. To decipher the antibacterial mechanism and promotion of wound healing activity by hydrogels embedded with biogenic Ag@ZnO core-shell nanocomposites. Chem Eng J. 2021;417;128025.
DOI: 10.1016/j.cej.2020.128025.